THE ASTROPHYSICAL JOURNAL, 447:829–847, 1995 July 10


# THE PHYSICS OF EARLY NOVA SPECTRA

PETER H. HAUSCHILDT AND SUMNER STARRFIELD
Department of Physics and Astronomy, Arizona State University, Box 871504, Tempe, AZ 85287-1504;
yeti@sara.la.asu.edu and starrfie@hydro.la.asu.edu

STEVEN N. SHORE
Department of Physics and Astronomy, Indiana University South Bend, 1700 Mishawaka Avenue, South Bend, IN 46634-7111;
sshore@paladin.iusb.indiana.edu

FRANCE ALLARD
Department of Geophysics and Astronomy, University of British Columbia, Vancouver, B.C., V6T 1Z4, Canada;
allard@astro.ubc.ca

AND

E. BARON
Department of Physics and Astronomy, University of Oklahoma, 440 West Brooks, Room 131, Norman, OK 73019-0225;
baron@phyast.nhn.uoknor.edu
*Received 1994 October 11; accepted 1995 January 24*

## ABSTRACT

We discuss the physical effects that are important for the formation of the early spectra of novae. Nova atmospheres are optically thick, fast expanding shells with flat density profiles, leading to geometrically very extended atmospheres. We show that the properties of early nova spectra can be understood in terms of this basic model and discuss some important effects that influence the structure and the emitted spectrum of nova atmospheres, e.g., line blanketing, non-LTE effects, and the velocity field. The proper modeling of nova atmospheres is discussed, and we give some computational details.

*Subject headings:* novae, cataclysmic variables — radiative transfer — stars: atmospheres

## 1. INTRODUCTION

The modeling and analysis of early nova spectra has made significant progress during the last 2–3 years by the construction of detailed model atmospheres and synthetic spectra for novae by Hauschildt et al. (1992, 1994a, b). In the early stages of the nova outburst, the spectrum is formed in an optically *very* thick, in both lines and continua, shell with a flat density profile, leading to very extended continuum and line-forming regions (hereafter, CFR and LFR, respectively). Because of the large variation of the physical conditions inside the spectrum-forming region, the classical term "photosphere" is not appropriate for novae. The large geometrical extension leads to a very large electron temperature gradient within the CFR and LFR, allowing for the observed simultaneous presence of several ionization stages of many elements. Typically the relative geometrical extension $R_{out}/R_{in}$ of a nova atmosphere is $\approx 100 \ldots 1000$, which is much larger than the geometrical extensions of hydrostatic stellar atmospheres (even in giants $R_{out}/R_{in}$ is typically less than 2) or supernovae (SNs). Nova atmospheres are also very different from SN atmospheres with respect to their energy balance. Whereas SNs spectra show constantly decreasing color temperatures and decreasing bolometric luminosities, the color temperatures of nova atmospheres generally increase with time and their bolometric luminosity is constant. This is caused by the presence of a central energy source in novae (the hot white dwarf) which is missing in SNs (where the only sources of energy are the radioactive decays Ni and Co nuclei).

For very low effective temperatures, molecules are present in the nova atmosphere. Therefore, the equation of state (EOS) in nova atmospheres is very complicated and special techniques must be employed so that nova model atmospheres can be constructed. The electron temperatures and gas pressures typically found in nova photospheres lead to the presence of a large numbers of spectral lines, predominantly Fe-group elements, in the LFR and a corresponding influence of line blanketing on the emergent spectrum. The situation is complicated significantly by the velocity field of the expanding shell which leads to an enhancement of the overlapping of the individual lines. This in turn makes simplified approximate treatments of the radiative transfer by, e.g., the Sobolev-approximation, very inaccurate and more sophisticated radiative transfer methods, which treat the overlapping lines and continua simultaneously, must be used in order to obtain reliable models. The line blanketing also leads to strong wavelength redistribution of the radiative energy, therefore, the temperature structure of the shell must be calculated including the effects of the line blanketing.

The situation is further complicated by the fact that the (electron) densities of the CFR and LFR in a nova atmosphere are very low compared to classical stellar atmospheres. This leads to an overwhelming dominance of the radiative rates over the collisional rates. In addition, the radiation field is very nongray. These two effects lead to large departures from local thermodynamic equilibrium (LTE) in the CFR and LFR. Therefore, non-LTE effects must be included self-consistently in the model construction, particularly in the calculation of the temperature structure and the synthetic spectra. As discussed in the previous paragraph, the effect of the line blanketing on the radiative rates requires a careful treatment of the radiative transfer in the non-LTE calculations and simple approximations can lead to wrong results.

In this paper, we will discuss the physics of the early nova spectrum in some detail with an eye to the inverse problem of understanding the evolution of the color temperatures of the observed spectra as a function of time. In the following section,

we describe the model assumptions, parameters, equations, and model construction. In § 3, we discuss some of the most important features of nova atmospheres, in particular, the structure of the atmosphere, the effect of line blanketing on the spectrum, the effects of different velocity fields on the spectrum, and non-LTE effects. We conclude the paper with a discussion of the results.

## 2. MODELING NOVA ATMOSPHERES AND SPECTRA

### 2.1. *Model Assumptions*

#### 2.1.1. *Nova Specific*

Following the discussion of Bath & Shaviv (1976), we consider nova photospheres to be spherical and expanding but stationary configurations. Therefore, we assume that all time-dependent terms both in the hydrodynamics and in the radiative transfer equation can be neglected and all quantities depend only upon the radial coordinate (except for the specific intensity of the radiation field which, in addition, depends on the angle to the radial direction). These assumptions are justified since the hydrodynamic timescale is much longer than the timescales for photon thermalization and for the establishment of excitation and ionization equilibria. The assumption of spherical symmetry is only an approximation, as all novae eject nonspherical and clumpy shells. However, in the early stages of the nova outburst the clumps are still very close together and the gas between the individual clumps will be optically thick. A three-dimensional treatment of the full problem is presently not feasible and simple approximations, e.g., neglecting non-LTE effects and/or line blanketing will lead to wrong conclusions.

Using the results from hydrodynamic calculations of the consequences of thermonuclear runaways in accreted envelopes on white dwarf stars (see Shara 1989; Starrfield 1989 for reviews), we assume that the density varies according to a power law, $\rho \propto r^{-N}$. For the earliest, fireball, phase of the nova outburst, the parameter $N$ is of the order of 15, a value typical for supernova envelopes. In later phases, the value of $N$ is much smaller, around 3, leading to very large geometrical extensions of nova atmospheres. We treat the velocity field as a free parameter, to be derived from the observed spectrum. In general, the velocity field can be either ballistic $v \propto r$ (in the fireball phase), or corresponding to $\dot{M}(r) = \text{const.}$ (in the wind phase). Depending on the density structure, the velocity field may also follow a standard "wind" profile, i.e., $v(r) = v_\infty(1 - a/r)^b$ with three free parameters $v_\infty$, $a$, and $b$, to be derived from the spectrum. In our model construction, we can allow for all three of the above velocity profiles (in fact, the only restriction posed on the velocity field is monotony).

We compute the temperature structure from the condition of radiative equilibrium in the co-moving frame. Radioactive decays do not have a significant influence on the temperature structure for atmospheres with $N \geq 3$ (Pistinner et al. 1995). For smaller $N$, radioactive energy deposition could have an influence on the temperature structure. Nonthermal excitation of lines and continua by fast primary and secondary electrons, however, may be important in the wind phase of the nova outburst and could help to explain some of the observed features. This is currently under investigation.

#### 2.1.2. *General*

The complicated interaction of overlapping lines and continua as well as the velocity field present in the LFR require a sophisticated treatment of the radiative transfer in the nova atmosphere. We, therefore, solve the full special relativistic nongray equation of radiative transfer (RTE) for both lines and continua. The maximum velocities typically found in novae would, in principle, allow us to restrict the radiative transfer to a complete first order in $\beta = v/c$; however, this restriction would not simplify the calculations (see below). Neglecting the advection and aberration terms, which are of order $\beta$, would lead to errors of $\approx 5\beta$ in the mean intensity (Mihalas et al. 1976; Hauschildt & Wehrse 1991). At maximum observed velocities of $\approx 5000$ km s$^{-1}$, this corresponds to errors of $\approx 8\%$ in the mean intensity $J$, which could lead to significant changes in the radiative rates and observable changes in the emergent spectra. Therefore, we choose to solve the full special relativistic RTE as described below. In addition, we solve the radiative energy equation in the Lagrangian frame including all velocity terms so that the temperatures structure is fully self-consistent with the radiation field.

The low densities and complicated radiation fields in the atmosphere require that the most important species are treated using multilevel non-LTE. At present, we can treat H I (15 levels), He I (11 levels), He II (15 levels), Na I (3 levels), Mg II (3 levels), Ca II (5 levels), and Ne I (26 levels) in non-LTE. We are currently working on including Fe II in non-LTE using a 617 level model atom with 13675 permitted transitions that are self-consistently included in the radiative transfer and statistical equilibrium calculations and will report the results of these calculations elsewhere (Hauschildt & Baron 1995).

The neon model atom was adapted from the model atom of Auer & Mihalas (1973). The energy levels were taken from Moore (1971), and the oscillator strengths from Auer & Mihalas (1973) and Murphy (1968). The photoionization cross sections were fitted from the data of Topbase 0.5 (Cunto & Mendoza 1992). The bound free collisional cross sections were fit to the semi-empirical formula of Drawin (1961)

$$\sigma(E) = \pi a_0^2 (I_H/E_n)^2 \left[ \alpha_0 \ln(x)/x + \sum_1^3 \alpha_i x^{-i} \right]$$

where $I_H = 13.6$ eV is the ionization energy of hydrogen, $E_n$ is the threshold energy of the transition, $a_0$ is the Bohr radius, and $x = E/E_n$. The coefficients are $\alpha = (2.99, -0.73, 1.22, 1.95)$. The bound-bound collision cross sections were scaled to the data of Hertz (1969), Sharpton et al. (1970), and Vajnshtejn & Minaeva (1968). For allowed transitions Van Regemorter's (1962) formula was used and within multiplets Allen's (1973) semi-empirical formula was used.

Our equation of state includes up to 26 ionization stages of 39 elements as well as 105 molecules (see Table 1). It was initially developed by Allard (1990) for use in M dwarf calculations (see also Allard & Hauschildt 1995) and is both versatile and numerically extremely stable. The large number of ionization stages is required to span the wide range of electron temperatures and gas pressures encountered in nova atmospheres (see below). For effective temperatures larger than $\sim 15{,}000$ K, molecules can be safely neglected, resulting in a much simpler EOS.

We include in the model calculations the most relevant *b-f* and *f-f* processes with the cross sections given in the compilation of Mathisen (1984). As stated above, line blanketing is a very important factor in the computation of nova model atmospheres. Therefore, we include the most important $\approx 2 \times 10^6$ lines dynamically selected from the list of $42 \times 10^6$ lines of Kurucz (1993a); for details of the selection process see

TABLE 1

MOLECULES CONSIDERED IN THE EOS

| | | | | | | | | | |
|---|---|---|---|---|---|---|---|---|---|
| $CS^-$ | $SiH^-$ | $OH^-$ | $H_2^-$ | $CH^-$ | $HS^-$ | $C_2^-$ | $CN^-$ | $BO^-$ | $FeO^-$ |
| $NO^+$ | OH | CH | NH | $C_2$ | CN | CO | MgH | CaH | SiH |
| TiO | $H_2O$ | $H_2$ | $N_2$ | NO | $CO_2$ | $O_2$ | ZrO | VO | MgS |
| SiO | AlH | HCl | HF | HS | TiH | AlO | BO | CrO | LaO |
| MgO | ScO | YO | SiF | NaCl | CaOH | HCN | $C_2H_2$ | $CH_4$ | $CH_2$ |
| $C_2H$ | HCO | $NH_2$ | LiOH | $C_2O$ | AlOF | NaOH | MgOH | $AlO_2$ | $Al_2O$ |
| AlOH | $SiH_2$ | $SiO_2$ | $H_2S$ | OCS | KOH | $TiO_2$ | TiOCl | $VO_2$ | $FeF_2$ |
| $YO_2$ | $ZrO_2$ | BaOH | $LaO_2$ | $C_2H_4$ | $C_3$ | $SiC_2$ | $CH_3$ | $C_3H$ | $NH_3$ |
| $C_2N_2$ | $C_2N$ | $CaF_2$ | AlOCl | $Si_2C$ | $CS_2$ | $CaCl_2$ | AlF | CaF | $Si_2$ |
| SiS | CS | AlCl | KCl | CaCl | TiS | TiCl | SiN | AlS | $AL_2$ |
| FeO | SiC | $TiF_2$ | FeH | LiCl | | | | | |

Hauschildt et al. (1992, 1994a, b). In order to allow for line scattering, which is important in low-density plasmas, we parameterize the albedo for line scattering using a parameter $\alpha$ (see also Kudritzki & Hummer 1990). In principle, $\alpha$ can be calculated only from a complete non-LTE calculations for all species, which is impractical. However, careful tests have shown that an average value of $\alpha = 0.95$ is appropriate for nova atmospheres and that changes in $\alpha$ do not alter the spectra significantly with the obvious exception of $\alpha = 0$ (full LTE) and $\alpha = 1$, which are both physically unreasonable. We include the effects of statistical (random) velocity fields using a Gaussian broadening velocity $\xi$. For most models presented here, we use $\xi = 50$ km s$^{-1}$ to simulate the effects of random small scale velocity fields on the intrinsic line widths. In test calculations we find that the models are not sensitive to the particular value of $\xi$ as long as it is significantly smaller than the expansion velocities.

At low electron temperatures molecular opacities become important. Therefore, we include collision-induced absorption (CIA) of $H_2$-$H_2$, $H_2$-H, and $H_2$-He, as well as more than 300 molecular bands of TiO, CN, OH, CH, CO, VO, MgH, SiH, CaH, and FeH if the molecular EOS is used. For very detailed modeling, we have the option of including molecular line blanketing by selecting the most important lines out of a list of $30 \times 10^6$ lines compiled from lists of Kurucz (1993b), Miller & Tennyson (Allard et al. 1994; $H_2O$), Jørgensen (Jørgensen & Larsson 1990; Jørgensen 1994; CN, TiO), the HITRAN92 database (Rothman et al. 1992), and Goorvitch (1994; CO). Details of the molecular bands and lines can be found in Allard & Hauschildt (1994). However, while molecular opacities become important for nova atmospheres with effective temperatures below $\sim 10{,}000$ K, they dominate for lower $T_{\rm eff}$.

### 2.2. *Model Parameter*

We choose as a numerically convenient set of basic parameters the effective temperature $T_{\rm eff}$, the luminosity $L$, and the density exponent $N$. The effective temperature is not well defined for extended atmospheres, our definition is based on $L = 4\pi R^2_{\tau_{\rm std}=1}\,\sigma T^4_{\rm eff}$. Here, $R_{\tau_{\rm std}=1}$ is the reference radius at $\tau_{\rm std} \equiv \tau_{5000\,{\rm A,cont}} = 1$. This parameterization of nova atmospheres was recently discussed by Pistinner et al. (1995). The velocity field inside the atmosphere is parameterized by either prescribing a radius-independent mass-loss rate $\dot{M}$ or the maximum expansion velocity, $v_\infty$. The radial form of the velocity field is then given by either $\dot{M}(r) = $ const. or by assuming a velocity law. We report here calculations made for either a ballistic velocity law ($v \propto r$) or for "radiatively driven wind" velocity laws of the general form $v \propto v_\infty(1 - a/r)^b$.

For nova atmosphere models with $N \leq 3$ we also need to choose the total mass of the envelope by using a cutoff outer density $\rho_{\rm out}$. This is required simply because the integral $\int_0^\infty \rho(r)dr$ diverges for $N \leq 3$. Additional parameters are the albedo for line scattering (for lines that are not treated explicitly in non-LTE) and, of course, the elemental abundances.

### 2.3. *Radiative Transfer and Radiative Equilibrium*

The time-independent, special relativistic, spherically symmetric radiative transfer equation in the Lagrangian ("comoving") frame is given by (see Mihalas & Weibel-Mihalas 1984)

$$\gamma(\mu+\beta)\frac{\partial I}{\partial r} + \frac{\partial}{\partial \mu}\left\{\gamma(1-\mu^2)\left[\frac{(1+\beta\mu)}{r} - \gamma^2(\mu+\beta)\frac{\partial \beta}{\partial r}\right]I\right\} - \frac{\partial}{\partial \nu}\left\{\gamma\left[\frac{\beta(1-\mu^2)}{\tau} + \gamma^2\mu(\mu+\beta)\frac{\partial \beta}{\partial r}\right]\nu I\right\} + \gamma\left[\frac{2\mu+\beta(3-\mu^2)}{r} + \gamma^2(1+\mu^2+2\beta\mu)\frac{\partial \beta}{\partial r}\right]I = \eta - \chi I\,. \quad (1)$$

In equation (1), $\mu$ is the cosine of the angle between a ray and the direction normal to the surface, $\nu$ the frequency, $I = I(r, \mu, \nu)$ denotes the specific intensity at radius $r$ and frequency $\nu$ in direction arccos $\mu$ in the Lagrangian frame. The matter velocity $v(r)$ is measured in units of the speed of light $c$, $\beta(r) = v(r)/c$, and $\gamma$ is given by $\gamma = 1(1 - \beta^2)^{1/2}$. The sources of radiation present in the matter are described by $\eta = \eta(r, \nu)$ and $\chi = \chi(r, \nu)$ denotes the extinction coefficient. $\eta$ contains contributions from scattering terms proportional to the mean intensity $J$ of the form $\sigma\bar{J}$ (where $\bar{J}$ is the mean intensity averaged over the line profile) which are explicitly treated in the radiative transfer. The radiation fields derived from the solution of equation (1) incorporate all relativistic effects, in particular, advection and aberration. However, these effects are small in the models presented in this paper in contrast to the situation found in SN envelopes (Hauschildt, Best, & Wehrse 1991; Hauschildt & Wehrse 1991). In addition, the acceleration terms $\propto \partial\beta/\partial r$ are much more important in nova atmospheres than in high-speed stellar winds due to the presence of larger velocity gradients in the nova atmosphere.

For a combination of, e.g., thermal, electron scattering, and line sources the emissivity $\eta$ can be written as

$$\eta = \kappa B_\lambda(T) + \sigma_e J + \sum_{\rm lines} \kappa_l \varphi(\lambda) \int_0^\infty \varphi(\lambda) J(\lambda) d\lambda\,.$$

In nova atmospheres, the scattering terms due to both electron and line scattering are usually important in the CFR and LFR and must, therefore, be included consistently in the solution of the radiative transfer.

Equation (1) is a partial integro-differential equation of a boundary value problem in the radius $r$ and an initial value problem in the wavelength for the specific intensity. Our numerical solution of the radiative transfer equation is based on the method of operator splitting or "accelerated Λ-iteration" (ALI; Cannon 1973; Scharmer 1984; Olson, Auer, & Buchler 1987). We use a variant of the short-characteristic method (Hauschildt 1992a) to obtain the formal solution of equation (1) along the characteristic rays and then use a band-matrix approximation to the discretized Λ-operator as our choice of the approximate Λ-operator (ALO) used in the operator splitting method. The convergence rate using a diagonal ALO, even if it is the exact diagonal of the Λ-matrix, is still not very good. A tridiagonal ALO, however, results in much faster convergence, thus reducing the number of iterations of the ALI method and, typically, also reducing the CPU time required for the solution of the RTE. We have implemented a band-matrix representation of the discretized Λ-matrix (Hauschildt et al. 1994c) which leads to an optimum convergence rate and minimizes the computer time required for the numerical radiative transfer by using an *adaptive* bandwidth of the ALO matrix.

The time-independent radiation energy equation is obtained by integrating equation (1) over $\mu$ and $\nu$ can be written as (Mihalas & Weibel-Mihalas 1984)

$$\gamma\left[\frac{\partial H}{\partial r}+\beta\frac{\partial J}{\partial r}+\frac{1}{r}(2H+3\beta J-\beta K)+\gamma^2\frac{\partial\beta}{\partial r}(J+K+2\beta H)\right] = \int_0^\infty(\eta_\lambda-\chi_\lambda J_\lambda)d\lambda\,, \tag{2}$$

where $J=\frac{1}{2}\int_0^\infty\int_{-1}^1 I_\lambda\,d\mu\,d\lambda$ is the wavelength-integrated mean intensity and $H=\frac{1}{2}\int_0^\infty\int_{-1}^1\mu I_\lambda\,d\mu\,d\lambda$, and $K=\frac{1}{2}\int_0^\infty\int_{-1}^1\mu^2 I_\lambda\,d\mu\,d\lambda$ are the wavelength-integrated first and second moments of the specific intensity.

This equation is closely coupled to the hydrodynamic equations of the moving matter and, therefore, is best solved using a radiation-hydrodynamic method. However, in astrophysical applications the density structure of an expanding model atmosphere is often given by a previous hydrodynamic simulation. In this case, it is a reasonable approximation to assume radiative equilibrium in the Lagrangian frame, i.e., to assume that each element of material absorbs the same amount of radiative energy that it emits. The condition of radiative equilibrium equation in the Lagrangian frame is then simply given by

$$\int_0^\infty(\eta_\lambda-\chi_\lambda J_\lambda)d\lambda=0\,. \tag{3}$$

The equivalent condition for the wavelength integrated Eddington flux, $H$, can be written in the form (Mihalas & Weibel-Mihalas 1984):

$$\frac{\partial(r^2H)}{\partial r}+\beta\frac{\partial(r^2J)}{\partial r}+\frac{\beta}{r}r^2(J-K)+\gamma^2\frac{\partial\beta}{\partial r}r^2(J+K+2\beta H)=0\,, \tag{4}$$

with

$$\int_0^\infty\chi_\lambda S_\lambda\,d\lambda=\int_0^\infty\chi_\lambda\partial_\lambda\,d\lambda\,. \tag{5}$$

Our numerical solution of the special relativistic radiative equilibrium condition is based on the method discussed by Hauschildt (1992b), but we have now replaced the hybrid ALI-partial linearization temperature correction method by an improved version of the Unsöld-Lucy method as described in Allard (1990). This method is more efficient in terms of the number of iterations required for convergence, and it is easier to implement than the hybrid method. For the conditions found in novae, a full first-order approximation would be sufficient, however, the additional terms do not make the numerical treatment more complicated. As in the case of the radiative transfer, neglecting the first-order advection and aberration terms would lead to inconsistencies in the solution of the problem and thus possibly systematic errors.

### 2.4. *Rate Equations*

The non-LTE rate equations have the form (Mihalas 1978)

$$\sum_{j<i}n_j(R_{ji}+C_{ji})-n_i\times\left[\Sigma_{j<i}\left(\frac{n_j^*}{n_i^*}\right)(R_{ij}+C_{ji})+\Sigma_{j>i}(R_{ij}+C_{ij})\right]+\Sigma_{j>i}n_j\left(\frac{n_i^*}{n_j^*}\right)(R_{ji}+C_{ij})=0\,. \tag{6}$$

In equation (6), $n_i$ is the actual, non-LTE population density of level $i$ and the symbol $n_i^*$ denotes the so-called LTE population density of the level $i$, which is given by

$$n_i^*\equiv\frac{g_i}{g_\kappa}n_\kappa\frac{2h^3n_e}{(2\pi m)^{3/2}(kT)^{3/2}}\exp\left(-\frac{E_i-E_\kappa}{kT}\right). \tag{7}$$

Here $n_\kappa$ denotes the *actual*, i.e., non-LTE, population density of the ground state of the next higher ionization stage of the same element; $g_i$ and $g_\kappa$ are the statistical weights of the levels $i$ and $\kappa$, respectively. In equation (7), $E_i$ is the excitation energy of the level $i$ and $E_\kappa$ denotes the ionization energy from the ground state to the corresponding ground state of the next higher ionization stage. The actual, non-LTE electron density is given by $n_e$. The system of rate equations is closed by the conservation equations for the nuclei and the charge conservation equation (cf. Mihalas 1978).

The rates for radiative and collisional transitions between two levels $i$ and $j$ (including transitions from and to the continuum; see below) are given by $R_{ij}$ and $C_{ij}$, respectively. In our notation, the upward (absorption) radiative rates $R_{ij}$ $(i<j)$ are given by

$$R_{ij}=\frac{4\pi}{hc}\int_0^\infty\alpha_{ij}(\lambda)J_\lambda(\lambda)\lambda\,d\lambda\,, \tag{8}$$

whereas the downward (emission) radiative rates $R_{ji}(i<j)$ are given by

$$R_{ji}=\frac{4\pi}{hc}\int_0^\infty\alpha_{ji}(\lambda)\left[\frac{2hc^2}{\lambda^5}+J_\lambda(\lambda)\right]\exp\left(-\frac{hc}{k\lambda T}\right)\lambda\,d\lambda\,. \tag{9}$$

Here, $J$ is the mean intensity, $T$ the electron temperature, and $h$ is Planck's constant. $\alpha_{ij}(\lambda)$ is the cross section of the transition $i\rightarrow j$ at the wavelength $\lambda$. We outline the numerical method that we use to solve the rate equations in Appendix A.

### 2.5. *Model Computation*

We compute the nova atmosphere models and synthetic spectra with our code PHOENIX, version 4.9. PHOENIX per-

forms the model iterations in the following way: first we construct the radial grid corresponding to the prescribed optical depth grid by integrating the equation

$$\frac{dr}{d\tau_{\rm std}} = -\frac{1}{(\kappa_{\rm std} + \sigma_{\rm std})} \tag{10}$$

on a prescribed optical depth grid $\tau_{\rm std}$, where $\tau_{\rm std}$ is the optical depth in the continuum at a wavelength of 5000 Å. We set the maximum optical depth of the $\tau_{\rm std}$-grid so large, typically around $10^4$, that the atmosphere is fully thermalized at every wavelength and that, therefore, we can assume LTE at the inner boundary of the atmosphere. Note that the numerical quadrature requires the frequent solution of the non-LTE EOS with given $T_e$ and $b_i$ which vary with optical depth. This procedure is repeated at the beginning of each model iteration because, in the early stages of the model construction, the variation with depth of both the temperature and the departure coefficients may change significantly from iteration to iteration. After the computation of the radial grid is complete, a line selection algorithm is carried out and the selected lines are stored (see Hauschildt et al. 1994a for details). The radiative transfer equation is then solved for all wavelengths and optical depths and the "approximate rate operators" and the temperature correction quantities are constructed. The new radiation field is used to compute new values of the radiative rates for all transitions (line and continuum) treated in non-LTE. These and the new $[R^*_{ij}]$ operators are then used to solve the non-LTE rate equations and to obtain new values for the departure coefficients for all depths.

The model iterations are stopped if the relative errors in the radiative equilibrium conditions and the temperature corrections, as well as the corrections for the $b_i$'s, are less than $10^{-3}$. We have checked the convergence properties of this scheme by using different initial estimates for the temperature structure and the run of the departure coefficients and found that the scheme always leads to true convergence and avoids the very slow convergence of a $\Lambda$-iteration due to the properties of the operator splitting method we employ for the solution of the radiative transfer and rate equations. Typically, for a line-blanketed, non-LTE model atmosphere, we use $N_s = 50$ depth points logarithmically spaced between $\tau_{\rm std} = 10^{-10}$ and $\tau_{\rm std} = 10^3$, and $\sim$30,000 wavelength points from $\lambda = 20$ Å to $\lambda = 10^7$ Å. Depending upon the initial stratification, 15–25 iterations are required to satisfy both the energy conditions and the values of the departure coefficients to a relative accuracy better than $10^{-3}$.

In Table 2 we give for references the parameters of the models discussed in the following section.

TABLE 2

MODELS DISCUSSED IN SECTION 3

| $T_{\rm eff}$ | $N$ | $v_{\rm max}$ | Velocity Field |
|---|---|---|---|
| 5000..... | 3 | 500 | Ballistic |
| 5500..... | 3 | 500 | Ballistic |
| 10000..... | 3 | 2000 | Ballistic |
| 15000..... | 3 | 2000 | Ballistic |
| 15000..... | 3 | 2000 | Wind |
| 20000..... | 3 | 2000 | Ballistic |
| 25000..... | 3 | 1600 | Ballistic |
| 25000..... | 3 | 1600 | Wind |
| 25000..... | 3 | 2000 | Ballistic |

## 3. RESULTS

### 3.1. *Structure of Nova Atmospheres*

The structure of nova atmospheres is strongly affected by both the large temperature gradient and the low densities in the LFR. For low effective temperatures, molecules are important in the outer parts of the LFR; cf Figure 1. In this figure, we display the relative concentration $P_i/P_{\rm gas}$ of the 12 most important molecular species for a model with $T_{\rm eff} = 5000$ K. The LFR is dominated by molecular hydrogen and even triatomic molecules such as water vapor are abundant enough to influence the emergent spectrum. However, novae with such low effective temperatures are very hard to detect, because this very cool phase can only last for a few hours just at the end of the fireball phase or at the beginning of the wind phase.

In Figure 2 we show the concentration of atomic and ionic species in two nova model atmospheres with effective temperatures of 15,000 K (Fig. 2*a*) and 25,000 K (Fig. 2*b*). These plots show that multiple ionization stages of an element (e.g., oxygen) can be present simultaneously in the atmosphere. In fact, the O ionization sequence forms a number of nested "Strömgren spheres" in the atmosphere. For the model with $T_{\rm eff} = 15{,}000$ K hydrogen recombines in the LFR, due to the large electron temperature gradient. This demonstrates that nova atmospheres are *not* always scattering dominated, which changes the physics of the continuum and line formation significantly.

### 3.2. *Effects of Line Blanketing*

Line blanketing in the ultraviolet and optical spectral ranges is the dominant source of opacity in nova atmospheres. In Figure 3 we display synthetic spectra for models with $T_{\rm eff} =$ 10,000 K (Fig. 3*a*) and 25,000 K (Fig. 3*b*). The plots also show the spectra obtained by neglecting all but the non-LTE lines (dotted curve) and the blackbody energy distribution for the effective temperature. Line blanketing has an enormous impact on the spectrum emitted by the model with $T_{\rm eff} = 10{,}000$ K, in particular in the UV. Practically all lines in the UV are *absorption* lines, only a few regions of relative transparency in the "line haze" exist, e.g., the broad features at $\sim$1350, 1500, 1600, 2000, and 2640 Å. These appear as "emission" features, but are merely holes in the "iron curtain." In the optical spectral range the line blanketing is more localized in overlapping absorption and P Cygni lines, but the effect is by far not as strong as in the UV. At $T_{\rm eff} = 25{,}000$ K, the optical lines show marginally overlapping P Cygni profiles, this is also the case for the UV lines above $\approx$1500 Å. Below 1500 Å the lines are mostly in absorption and the spectrum is formed in a very similar way as the UV spectrum of the 10,000 K model. Note that some features change their character when the effective temperature increases. For example, the 2640 Å feature is for $T_{\rm eff} \approx 15{,}000$ K formed by a gap between strong Fe II lines, but at $T_{\rm eff} \approx$ 20,000 K it is formed by the overlapping emission parts of Fe II lines just shortward of 2640 Å.

Both models discussed here include $\sim$100,000 spectral lines, this is about the number of lines that are required to "saturate" the spectrum, i.e., the synthetic spectrum does not change significantly if more lines are included but would change considerably if fewer lines were used. We demonstrate this in Figure 4 which shows the effects of increasing the number of lines on the synthetic spectrum for a model with $T_{\rm eff} = 10{,}000$ K. Here, the model structure was taken from a fully self-consistent non-LTE model including $\approx$400,000 lines.

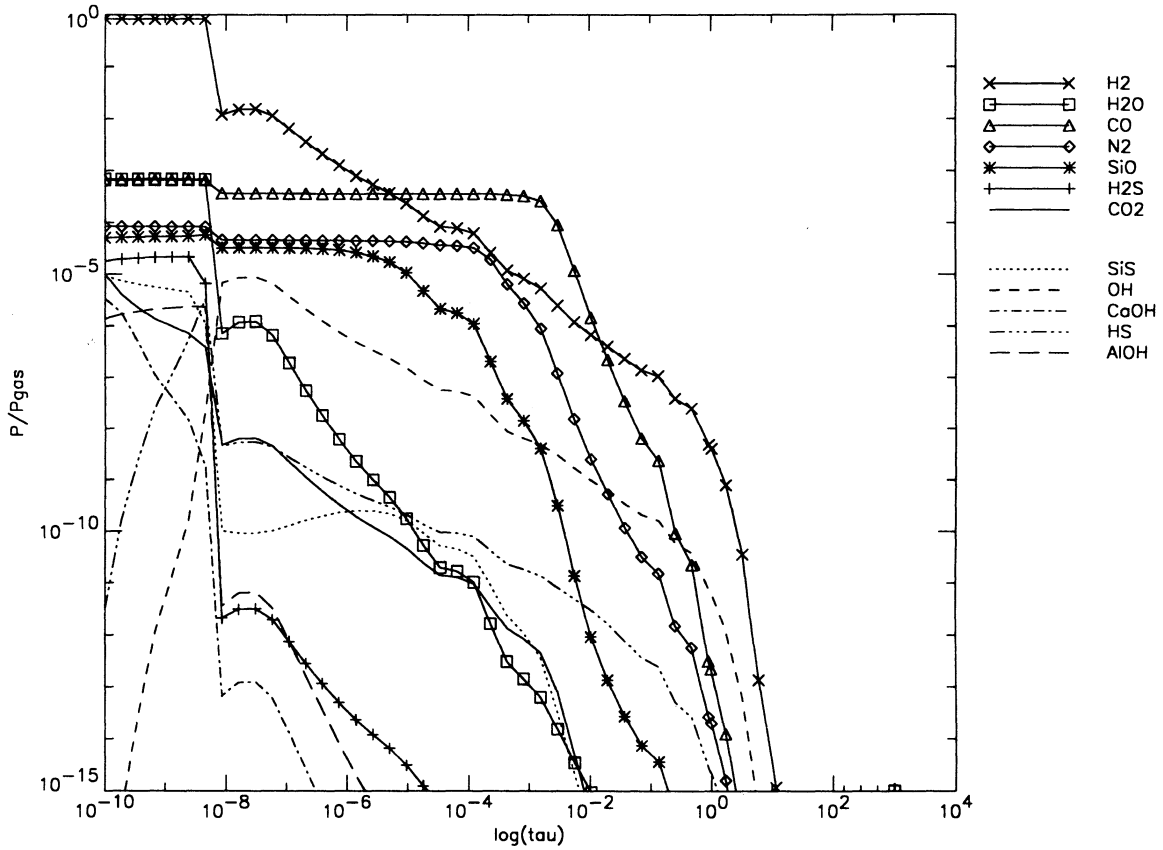


FIG. 1.—Relative concentration of molecular species in a nova atmosphere model with $T_{\rm eff} = 5000$ K, $N = 3$, and solar abundances. The plot gives the partial pressures of the indicated molecules relative to the gas pressure as functions of standard optical depth $\tau_{\rm std}$ (see text). In the outermost part of the atmosphere molecules are the dominant constituents but their concentration drops quickly with increasing $\tau_{\rm std}$ due to the increase in electron temperature.

The topmost panel shows the synthetic spectrum obtained by including only the non-LTE lines (in the plotted wavelength range, H I and Mg II) and the bottom panel shows the synthetic spectrum computed including more than 24 million lines. The synthetic spectra do not change significantly if more than ~100,000 lines are included in the calculation.

Figure 5 shows the effect of line blending for the Mg II $h + k$ doublet. The dotted line gives the pure Mg II profile, i.e., every line other than the $h + k$ lines is neglected, whereas the full curve gives the line profile calculated including other lines. The changes in the line profile are obvious and significant. Therefore, one must be very careful in analyzing observed nova line profiles and include blending in the analysis. We find that ~500,000 lines are stronger than $\sim 10^{-4}$ times the local absorptive continuum for $\xi = 50$ km s$^{-1}$. The vast majority of these lines have wavelengths smaller than 4000 Å, so that on the average 125 lines lie within 1 Å. This corresponds to an average spacing of 2.4 km s$^{-1}$ at 1000 Å, which is much smaller than the width of the individual lines, leading to a strong overlap. For $\xi = 2$ km s$^{-1}$, we find that $\sim 4.8 \times 10^6$ lines are stronger than $10^{-4}$ of the local continuum, i.e., their average spacing is ~0.25 km s$^{-1}$ so that they are also completely overlapping. The vast majority of these lines are relatively weak and form a slowly varying "pseudocontinuum" which serves as a background on which the few very strong lines form individual P Cygni profiles.

In Figure 6 we show the departure coefficients $b_i$ for two models with effective temperatures of 10,000 and 25,000 K, respectively. The ground state departure coefficient $b_1$ is annotated by the plus signs symbols for each species. It can be seen that the departures from LTE are large throughout both the LFR and the CFR. In addition, the $b_i$ can be both larger and smaller than unity, depending on the species, the level under consideration, and the optical depth. Typically we find that the $b_i$ are smaller than unity in the outer parts of the atmospheres. This is caused by the gaps in the line forest. In these gaps the mean intensity $J$ is larger than the local Planck-function $B$, thus leading to overionization and $b_i < 1$. Therefore, line blending has an *enormous* influence on the results of non-LTE calculations through the radiative rates. Hauschildt & Ensman (1994) discuss similar effects in supernova calculations. Neglecting line blanketing leads to much larger departures from LTE (the radiation field is super-Planckian in the outer atmosphere) which, in turn, leads to huge errors in abundance determinations. This means that a fully self-consistent solution of the non-LTE radiative transfer, rate, and energy equations, including line blanketing, is *necessary* in order to obtain reliable physical models of nova atmospheres.

The large deviation from a blackbody energy distribution and the extreme nongray spectrum cause a large effect of the lines on the temperature structure of nova atmospheres. This is illustrated in Figure 7 in which we compare the temperature structure of two models with $T_{\rm eff} = 10{,}000$ K and 20,000 K computed either with line blanketing (solid curves) or by neglecting line blanketing (dotted curves). The large effect of line cooling (in the optically thin regions) and back-warming

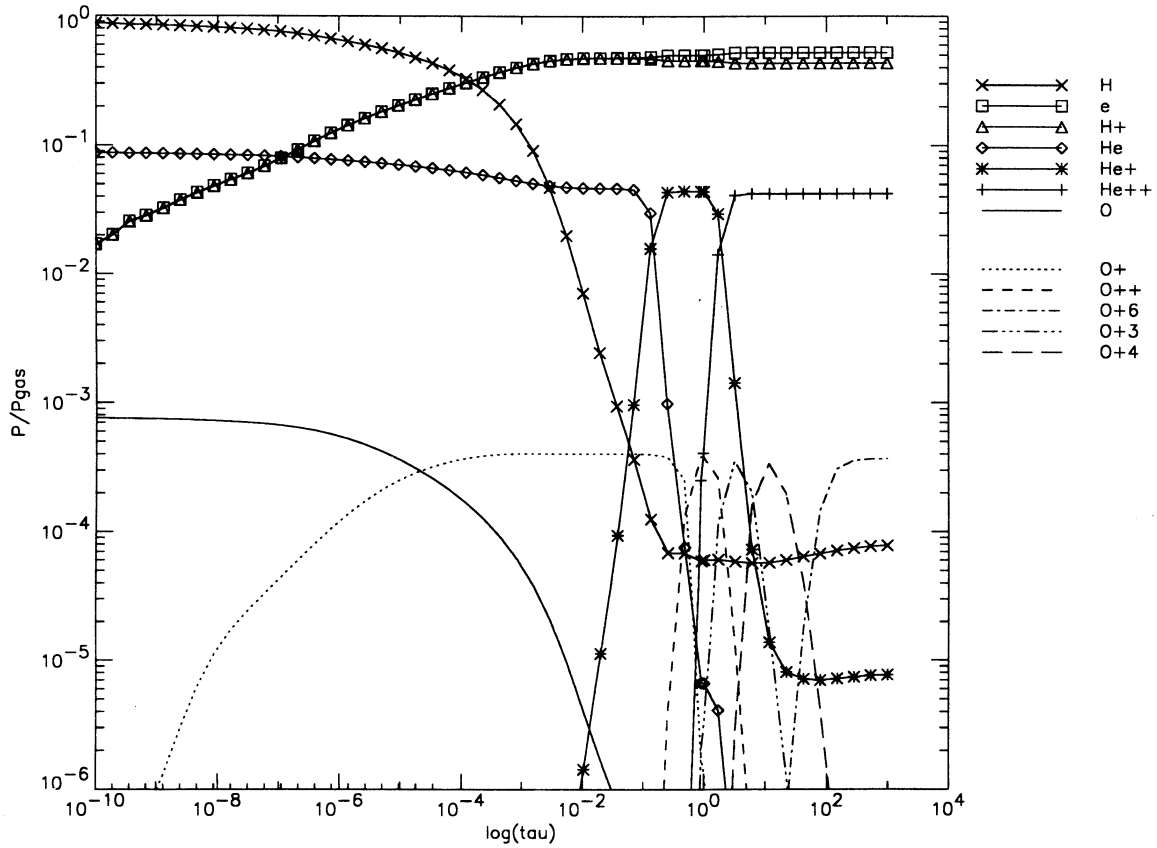


FIG. 2*a*

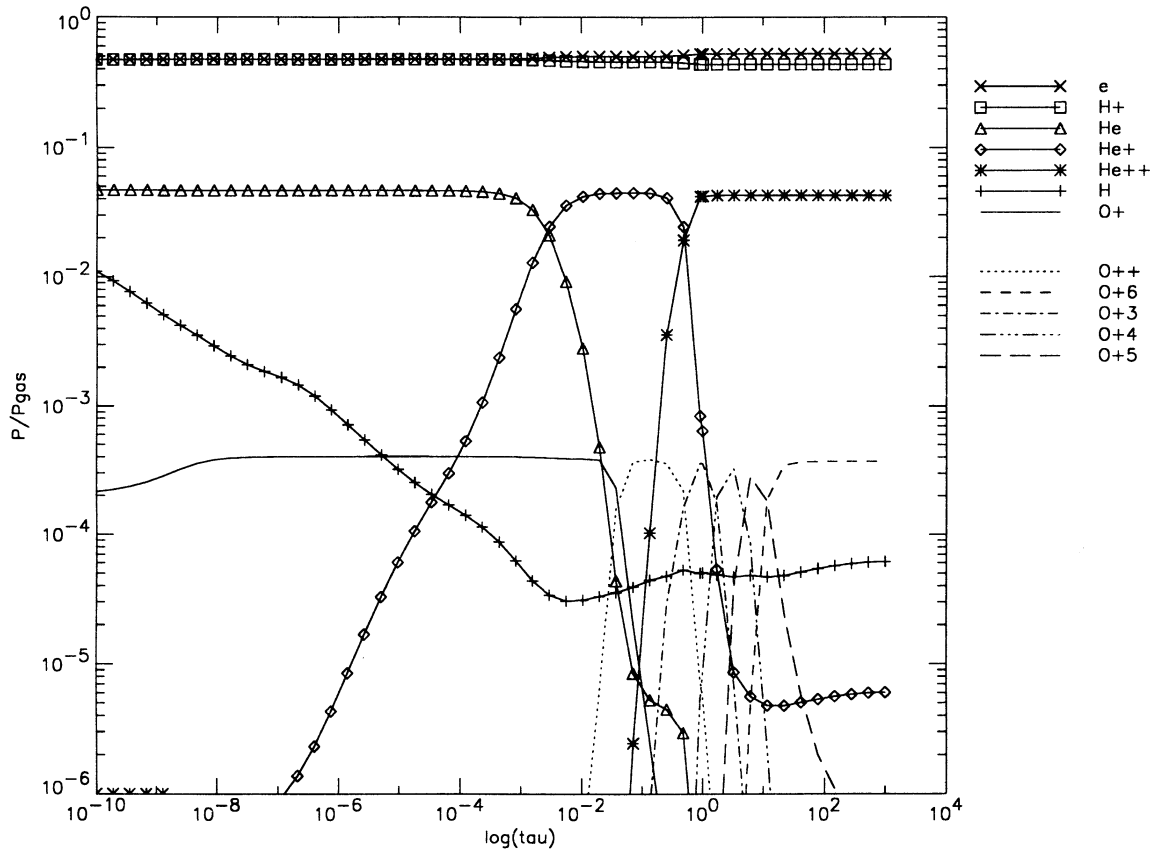


FIG. 2*b*

FIG. 2.—Relative concentration of atoms and ions in nova atmosphere models with (*a*) $T_{\rm eff}$ = 15,000 K, (*b*) $T_{\rm eff}$ = 25,000 K, $N$ = 3, and solar abundances. The plot gives the partial pressures of the indicated species relative to the gas pressure as functions of standard optical depth $\tau_{\rm std}$ (see text).

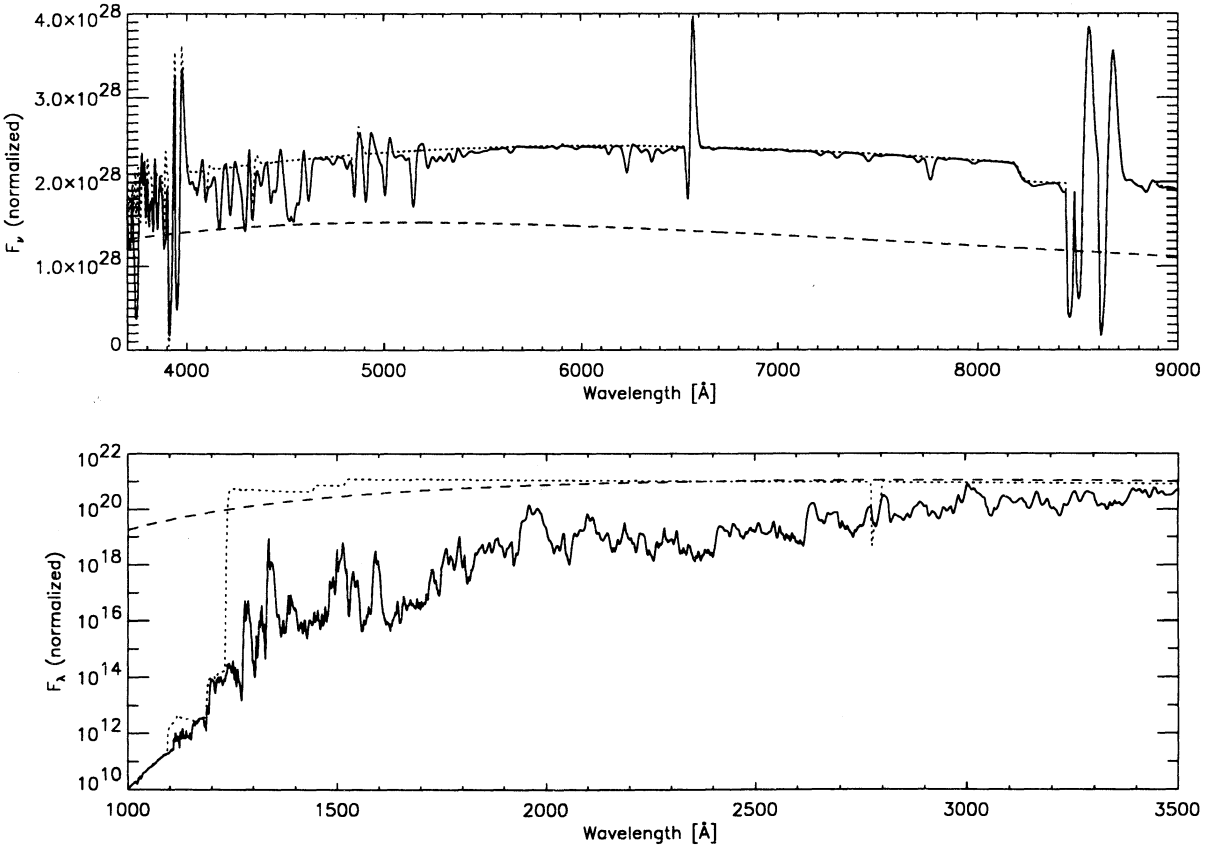


FIG. 3*a*

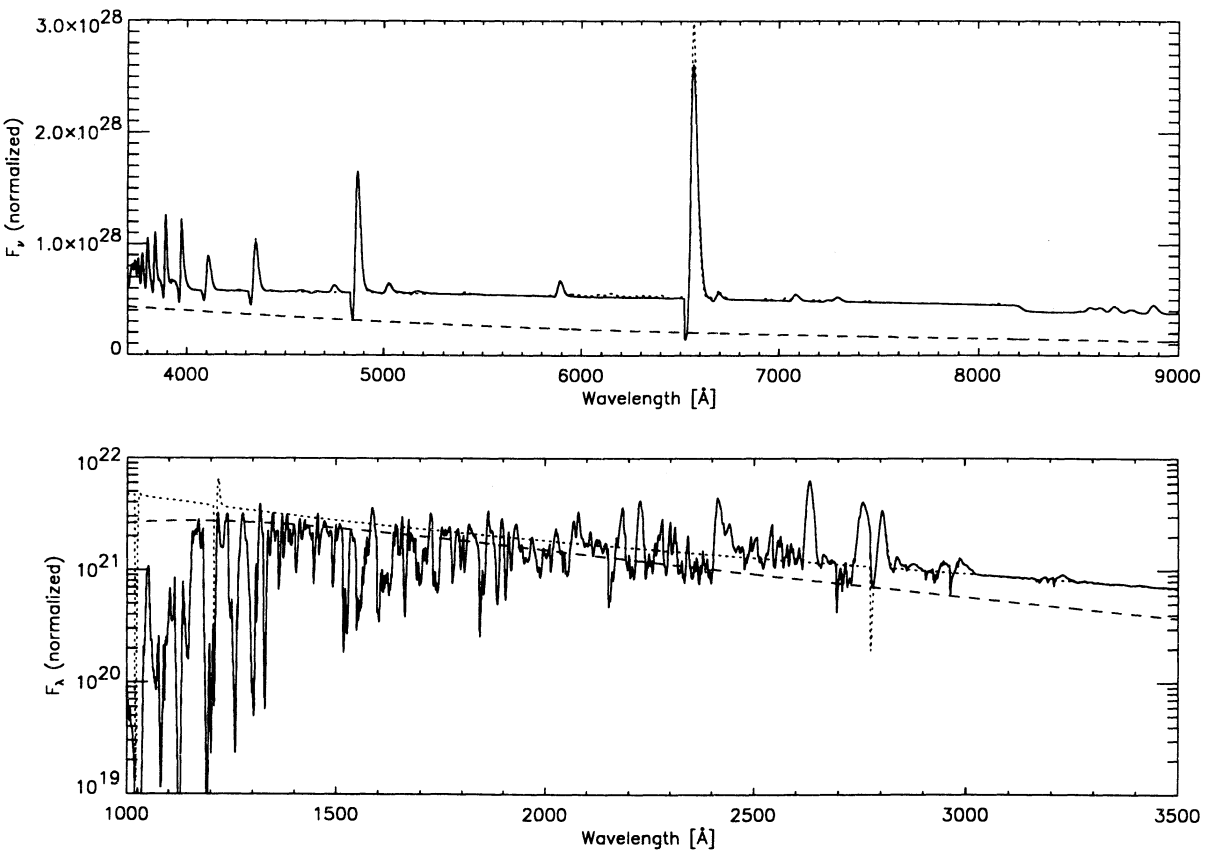


FIG. 3*b*

FIG. 3.—Effect of line blanketing on synthetic nova spectra. The plots show synthetic spectra computed with full line blanketing (*solid curves*), only non-LTE lines (*dotted curves*) and the blackbody energy distribution for models with $T_{\rm eff}$ = 10,000 K (*a*) and $T_{\rm eff}$ = 25,000 K (*b*) with $N$ = 3, and solar abundances. Note that the upper part of each plot gives $F_\nu$ in the optical on a *linear* scale, whereas the lower part gives $F_\lambda$ in the UV on a *logarithmic* scale.

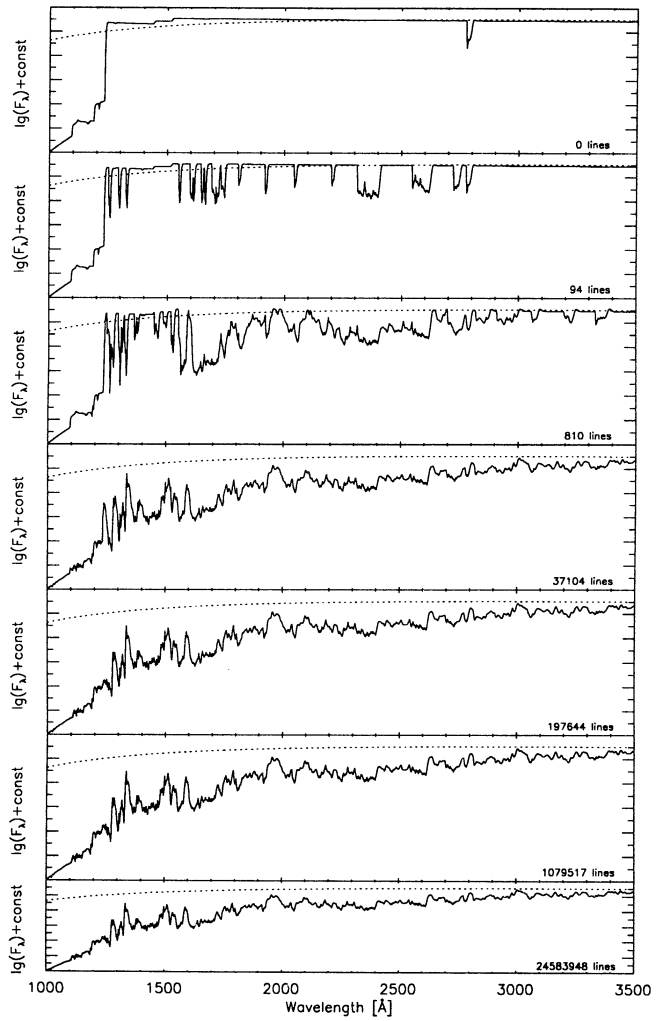


FIG. 4.—The effect of steadily increasing the line blanketing on synthetic nova spectra. The expanding, non-LTE nova model atmosphere has the parameters $T_{\rm eff} = 10{,}000$ K, $N = 3$, $v_{\rm max} = 2000$ km s$^{-1}$, and solar abundances. The calculation of the model atmosphere includes, self-consistently, non-LTE effects of H, Mg II, Ca II, He I, Na I, and Ne I (with 25 wavelength points per permitted non-LTE line) as well as line blanketing of $\sim$400,000 metal lines. In the uppermost panel, we display synthetic UV spectra in which only the non-LTE lines (here, the H I Lyman series and the Mg II $h + k$ doublet) have been included. The dotted line gives the blackbody energy distribution for $T = T_{\rm eff}$. The subsequent panels show synthetic spectra with an increasing number (roughly by a factor of 10 from panel to panel) of metal lines. The number of included metal lines is listed in each panel. These lines overlap strongly due to the differential expansion and form a "pseudocontinuum" (or the "iron curtain"). The figure shows the importance of an adequate treatment of metal line blanketing in modeling nova spectra during the early stages. Typically, $10^5$ lines are required and sufficient for accurate model construction and a synthetic spectrum.

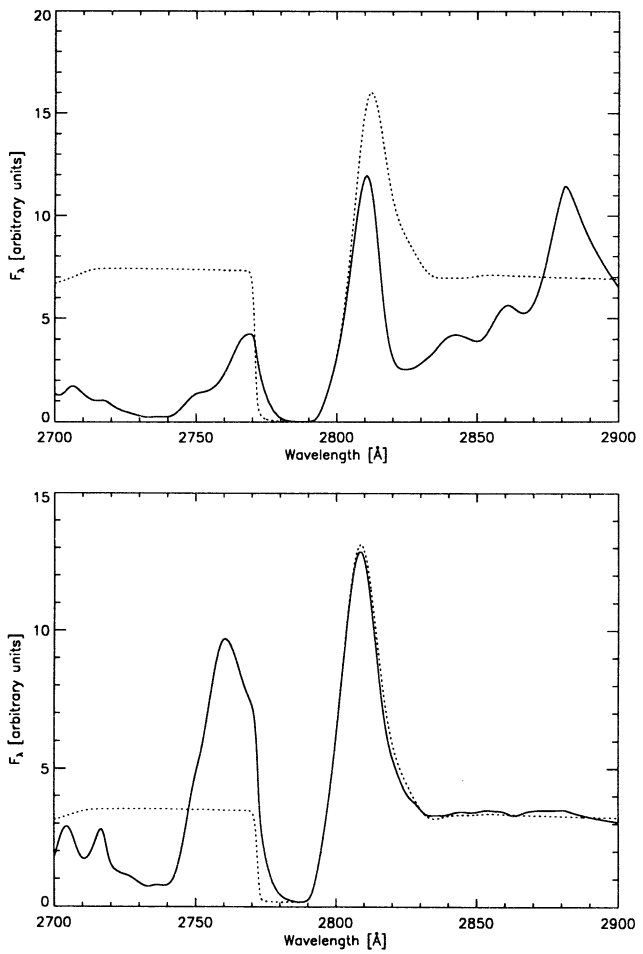


FIG. 5.—The region around the Mg II $h + k$ lines for two models with $T_{\rm eff} = 10{,}000$ K (*upper panel*) and $T_{\rm eff} = 15{,}000$ K (*lower panel*). The dotted curves give the spectrum obtained if line blanketing by Fe II lines is neglected, the solid curves give the synthetic spectra including Fe II line blanketing in addition to the Mg II lines. The significant changes of the Mg II $h + k$ line profiles due to overlapping Fe II lines is very apparent in this plot and demonstrates the importance of a proper treatment of overlapping lines in the model construction and the computation of synthetic spectra of novae.

(in the inner regions) is evident. The temperatures changes introduced by line blanketing can amount to more than 2000 K in the CFR and LFR, thus changing the synthetic spectra significantly. This demonstrates that a nova model atmosphere must include the line blanketing self-consistently in order to derive parameters, in particular elemental abundances, otherwise the results are unreliable. We show this in Figure 8 by comparing the synthetic spectrum calculated using a self-consistent non-LTE temperature structure (including line blanketing) to a spectrum calculated using the temperature structure of an LTE continuum model. The differences between the two spectra are dramatic and without the fully self-consistent calculation we would arrive at wrong conclusions about the parameters and, particularly, the abundances of the nova atmosphere.

### 3.3. *Color Temperatures*

In Figure 9 we show the color temperatures for three synthetic nova spectra as functions of wavelength. Here we define the color temperature $T_{\rm col}(\lambda_0)$ between two wavelengths $\lambda_0$ and $\lambda_1$ as the temperature of a blackbody energy distribution giving the same ratio $F_\lambda(\lambda_1)/F_\lambda(\lambda_0)$ as the synthetic spectrum. The curves in Figure 9 were computed using $\lambda_1 = \lambda_0 + 500$ Å and the fluxes at both wavelength points were averaged over $\pm 50$ Å. The figure shows that the color temperatures are highly variable with wavelength. The small-scale variations of $T_{\rm col}$ with wavelength are caused by the presence of the lines, we have smoothed the curves to minimize this effect. At smaller wavelengths, the color temperatures are much smaller than the effective temperature for $T_{\rm eff} < 20{,}000$ K, whereas in the optical spectra range they are comparable. In the IR, the color temperatures are again smaller than $T_{\rm eff}$ for $T_{\rm eff} > 15{,}000$ K.

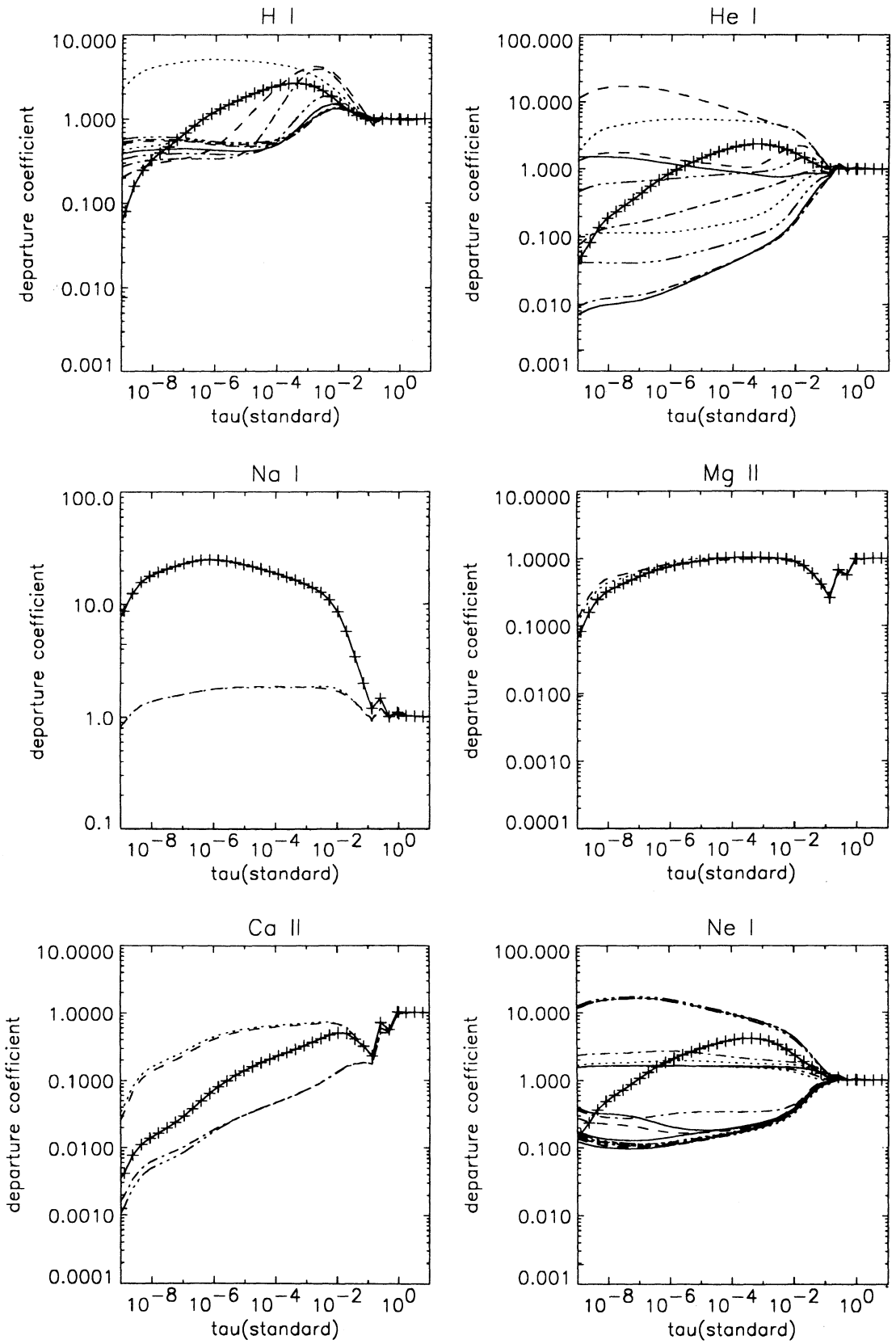


FIG. 6*a*

FIG. 6.—Departure coefficients $b_i$ as functions of standard optical depth $\tau_{std}$ for two nova atmosphere models with (*a*) $T_{eff}$ = 15,000 K and (*b*) $T_{eff}$ = 25,000 K. In each plot the departure coefficient of the ground state of the species is annotated by the plus signs.

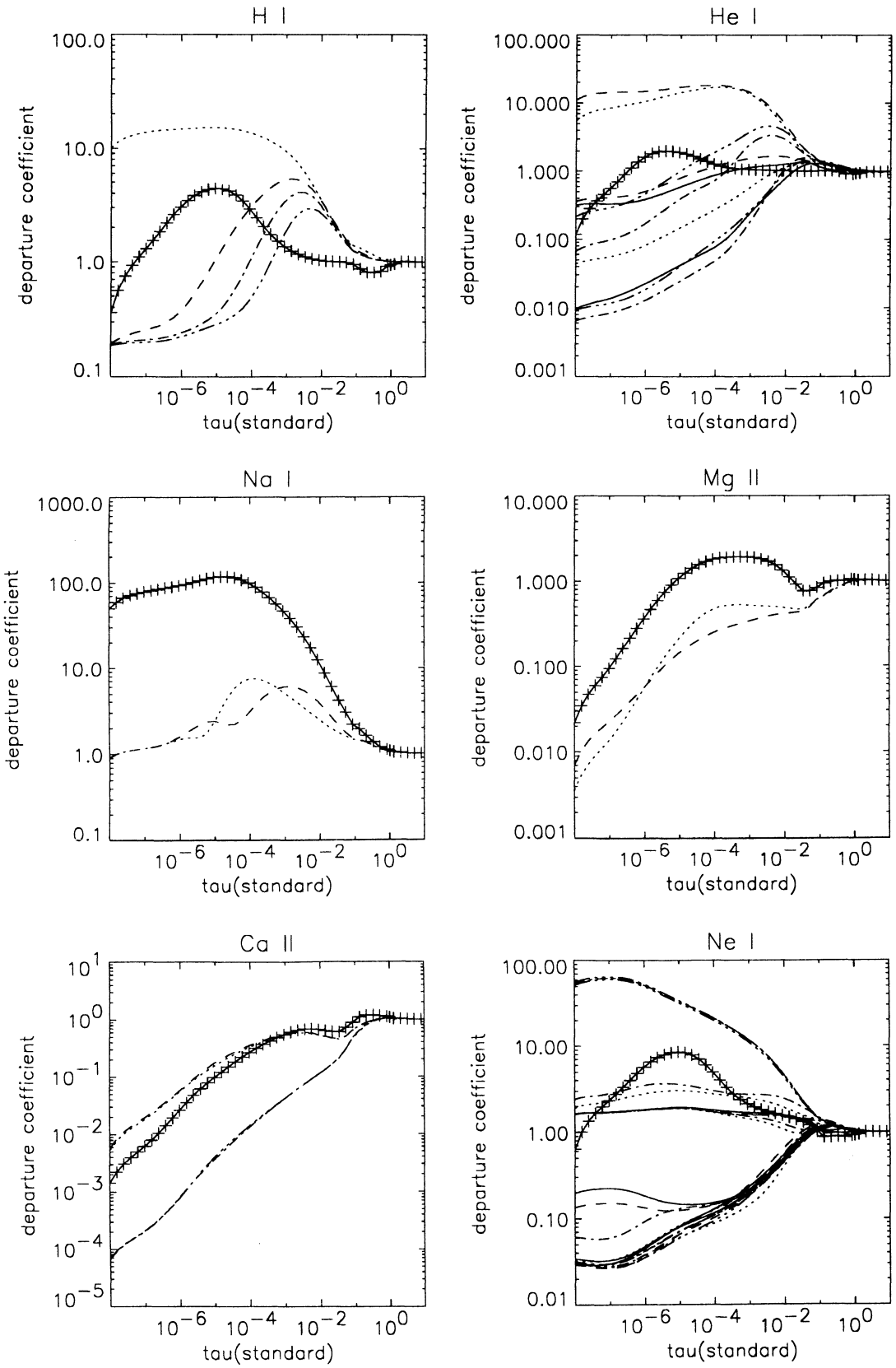


FIG. 6*b*

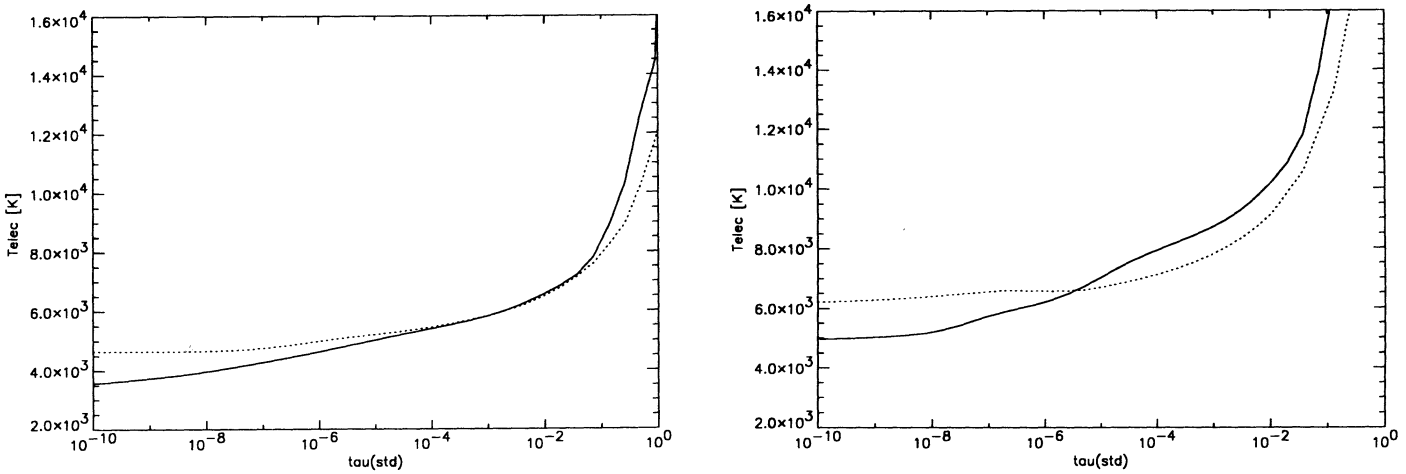


FIG. 7.—Effects of line blanketing on the temperature structure of nova atmospheres. The plots show the temperature structure computed including full line blanketing (*solid curves*) or neglecting lines (*dotted curves*) for models with $T_{\rm eff}$ = 10,000 K (*top panel*) and $T_{\rm eff}$ = 20,000 K (*bottom panel*) with $N$ = 3, and solar abundances.

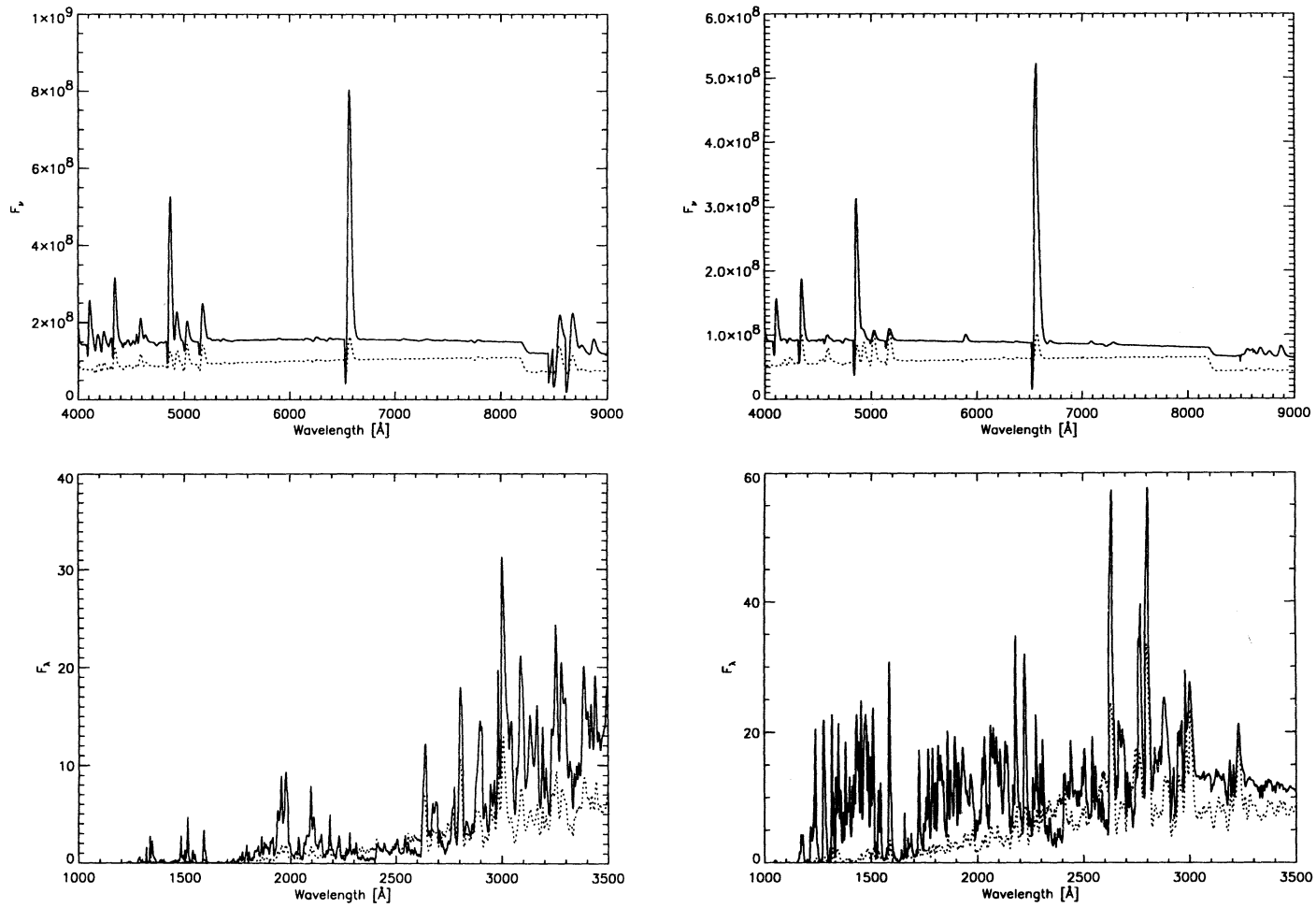


FIG. 8*a*

FIG. 8*b*

FIG. 8.—Effect of the temperature structure and non-LTE effects on the spectra of nova atmospheres. The plots show the synthetic spectra calculated using a fully self-consistent temperature structure including full line blanketing and non-LTE effects (*solid curves*) and computed using a temperature structure constructed neglecting line branketing and non-LTE effects (*dotted curves*) for models with (*a*) $T_{\rm eff}$ = 15,000 K and (*b*) $T_{\rm eff}$ = 20,000 K with $N$ = 3, and solar abundances.

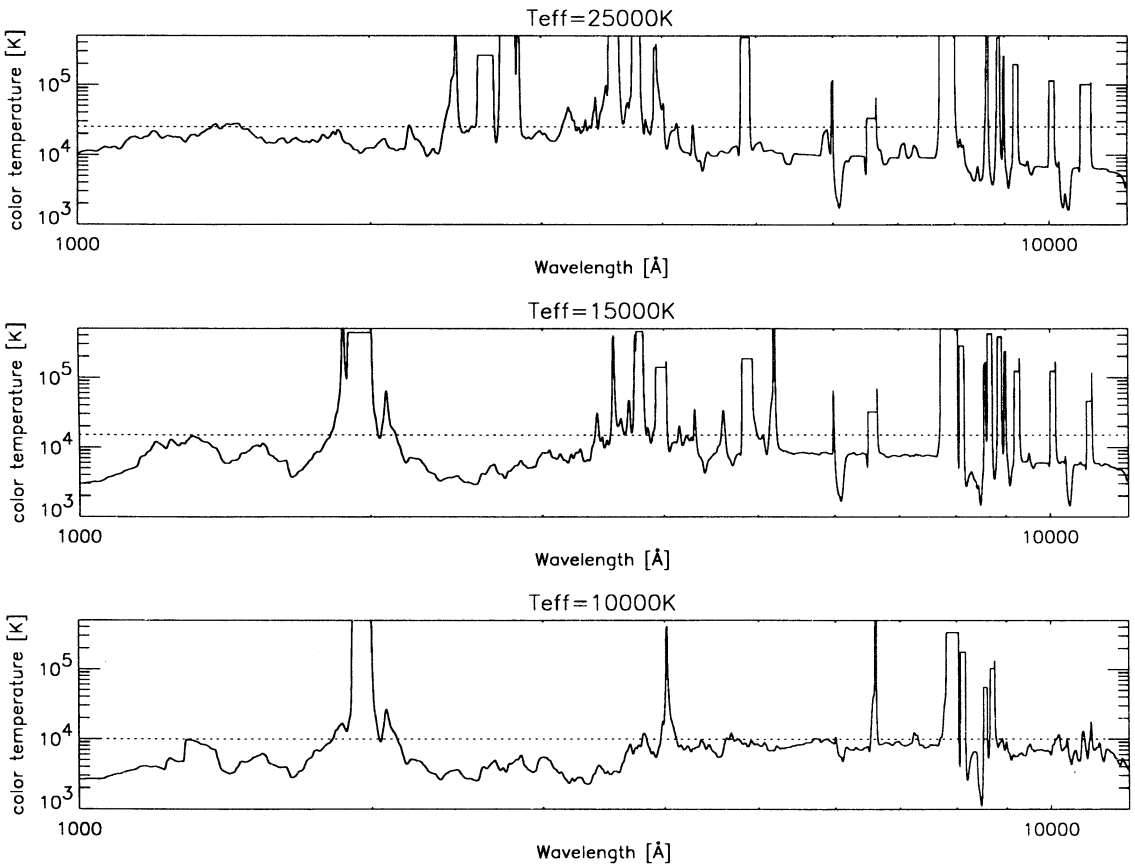


FIG. 9.—Color temperatures of synthetic nova spectra. The different panels give the color temperatures of synthetic nova spectra for three models with $T_{\rm eff}$ = 25,000 (*top panel*), 15,000 (*middle panel*), and 10,000 K (*bottom panel*) as function of the wavelengths. The color temperatures were computed using two wavelength points $\lambda$ and $\lambda$ + 500 Å, at each wavelength point the fluxes were averaged over ±50 Å. The strong variations are due to the effects of the lines, the dotted lines indicate the effective temperature of the corresponding model.

This shows again that nova spectra do not resemble blackbody energy distributions and that estimates of the effective temperatures based on color indices can be very misleading.

### 3.4. *Effects of the Form of the Velocity Field*

The form of the velocity field in the atmosphere also effects the emitted line profiles. We can use this additional information to derive the form of the velocity field from observed line profiles, which in turn indicates the ejection mechanism of the shell. In Figure 10 we compare synthetic spectra calculated using a ballistic (linear) velocity field (bottom spectrum in each plot) with spectra computed using a wind-type velocity law with $b = 0.1$ (top spectrum in each plot). All models have the same maximum velocity of 2000 km s$^{-1}$. Figure 10*a* shows the results obtained for models with $T_{\rm eff}$ = 15,000 K, whereas in Figure 10*b* a model with $T_{\rm eff}$ = 25,000 K is shown. The figures show that there are significantly different effects of the form of the velocity field on the optical and UV spectra. In the optical, the emission parts of the P Cygni profiles are broader and the absorption parts are narrower for the "wind" velocity field when compared to the ballistic velocity field. This is caused by the fact that for the optical lines the velocity gradient in the LFR of the "wind" velocity field is much smaller than in the ballistic case.

In the UV the effects are more pronounced than in the optical and different for the 15,000 K and the 25,000 K models. In the cooler model, the appearance of the UV spectrum changes significantly; the shapes of the different features are altered. This is caused by the different velocity gradients in the LFRs of the two models, which directly influences the amount of the overlap between lines. In the hotter model, the features remain essentially the same for both velocity laws, however, the "wind" velocity field model shows much more "fine structure" superimposed on the broader features. This general behavior makes the UV less attractive as a velocity field indicator for hotter nova atmospheres because the "fine-structure" can easily be confused with noise in the observed spectrum if the S/N and/or the resolution of the observations are not high enough.

### 3.5. *Effects of the Luminosity on the Spectrum*

The influence of different parameters chosen for the model construction on the synthetic spectra has been discussed in some detail by Pistinner et al. (1995). They found both the analytical and simplified numerical test calculations that some of the "classical" parameters may have only a marginal influence on the emitted spectrum and, therefore, cannot be determined from the spectrum. We demonstrate that this behavior is also true for full model atmosphere calculations of novae. As an example, we calculate the influence of the luminosity $L$, formally an input parameter, on the emergent spectrum (Fig. 11). All remaining parameters, in particular the outer density and the maximum expansion velocity, are identical in both models (note that, therefore, the model atmospheres with the

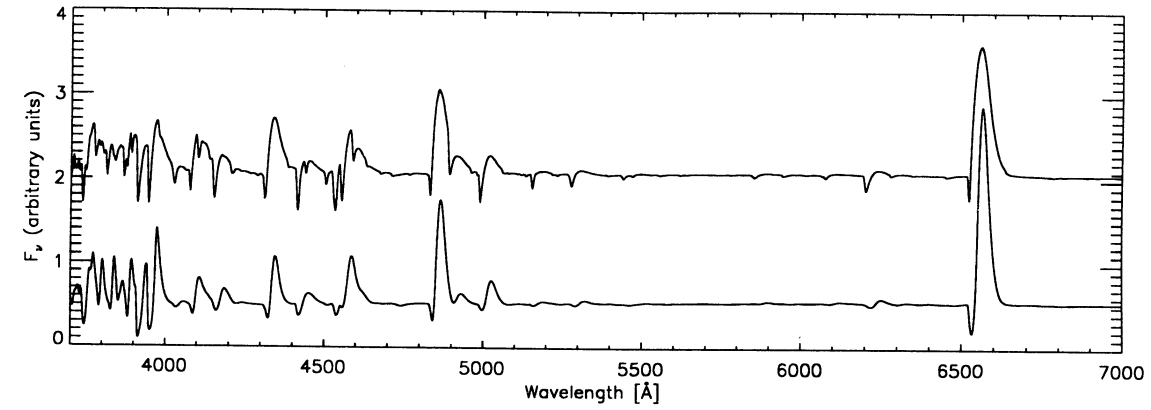


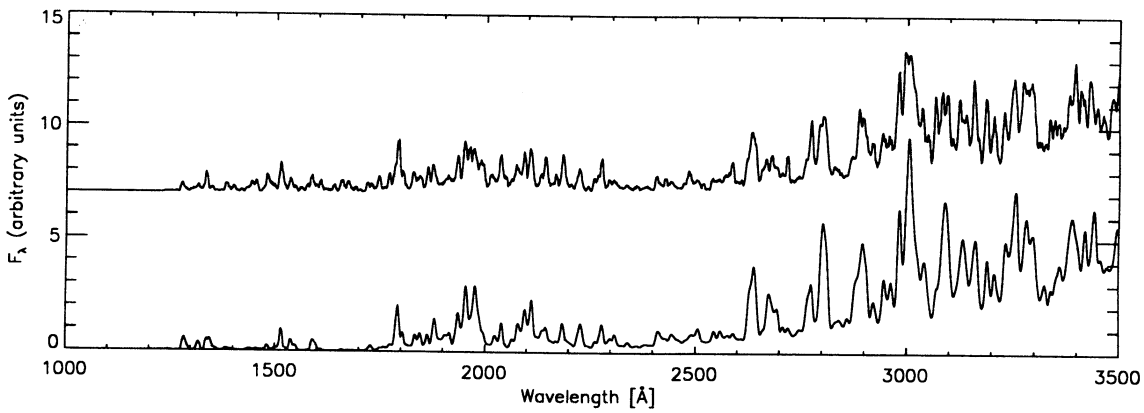


FIG. 10*a*

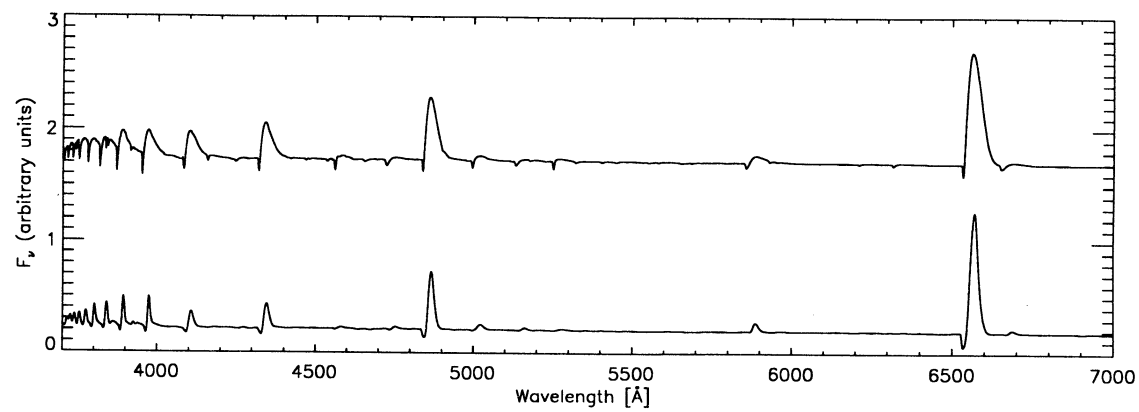


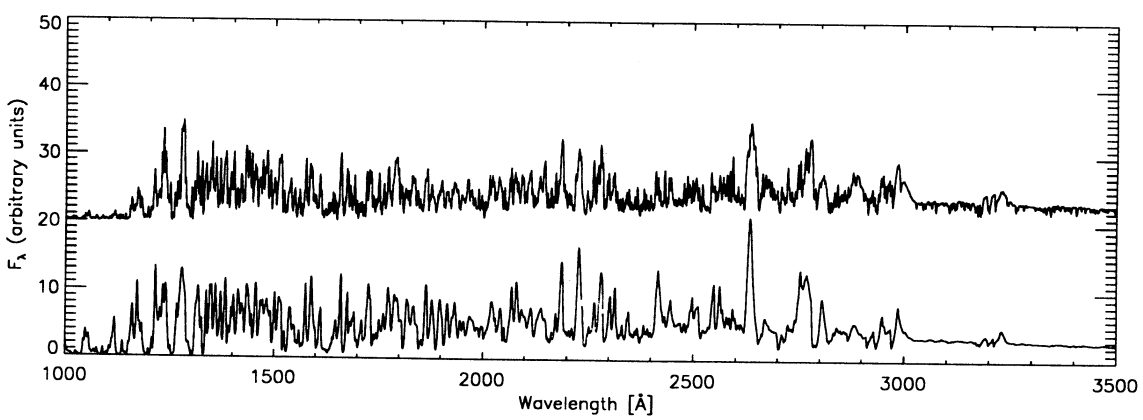


FIG. 10*b*

FIG. 10.—Effect of two different velocity laws on the spectrum of nova atmospheres. (*a*) The results for a model atmosphere with $T_{\rm eff} = 15{,}000$ K and $v_{\rm max} = v_\infty = 2000$ km s$^{-1}$ whereas panel (*b*) is for $T_{\rm eff} = 25{,}000$ K and $v_{\rm max} = v_\infty = 1600$ km s$^{-1}$. In each plot, the top curve is the spectrum calculated using a "wind" velocity field of the general form $v(r) \propto v_\infty(1 - a/r)^b$, whereas the bottom curve represents the results for the ballistic (linear) velocity law. Both models have the common parameter $N = 3$ and twice the solar metal abundances and are self-consistently calculated with their respective velocity fields.

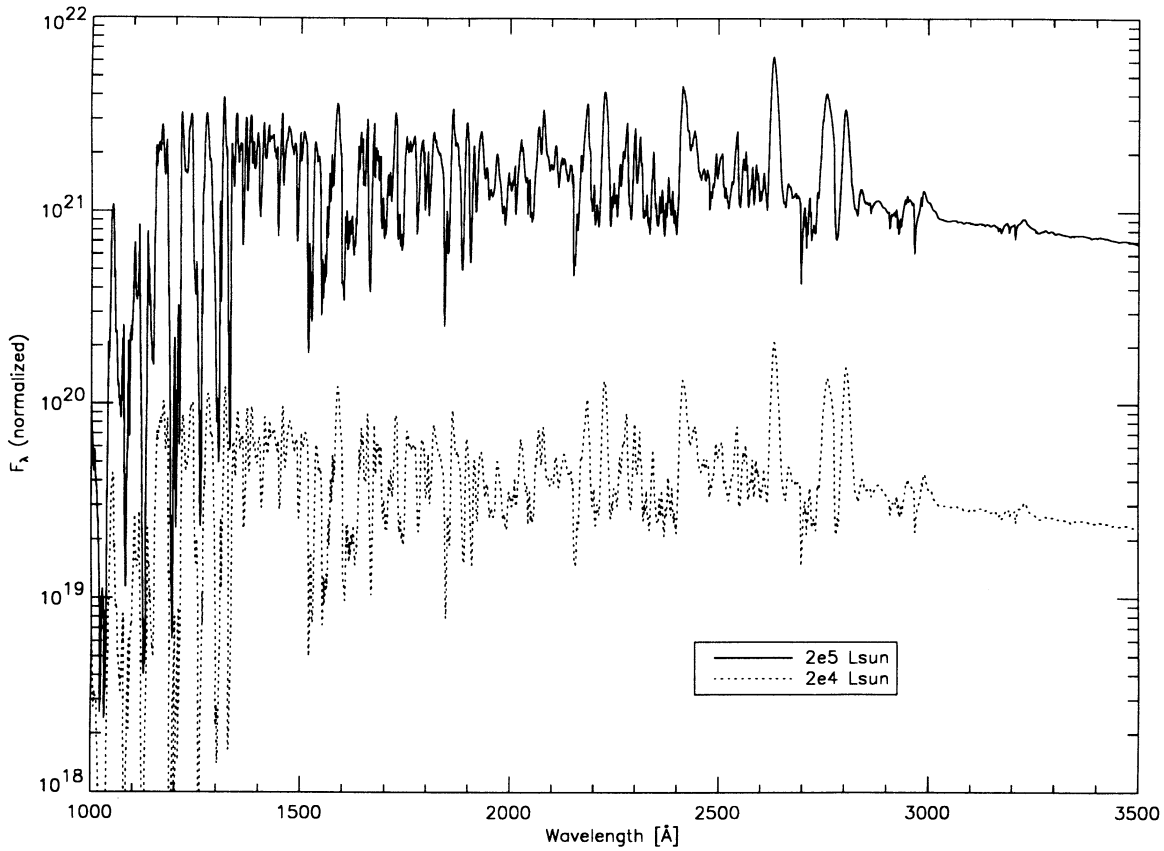


FIG. 11*a*

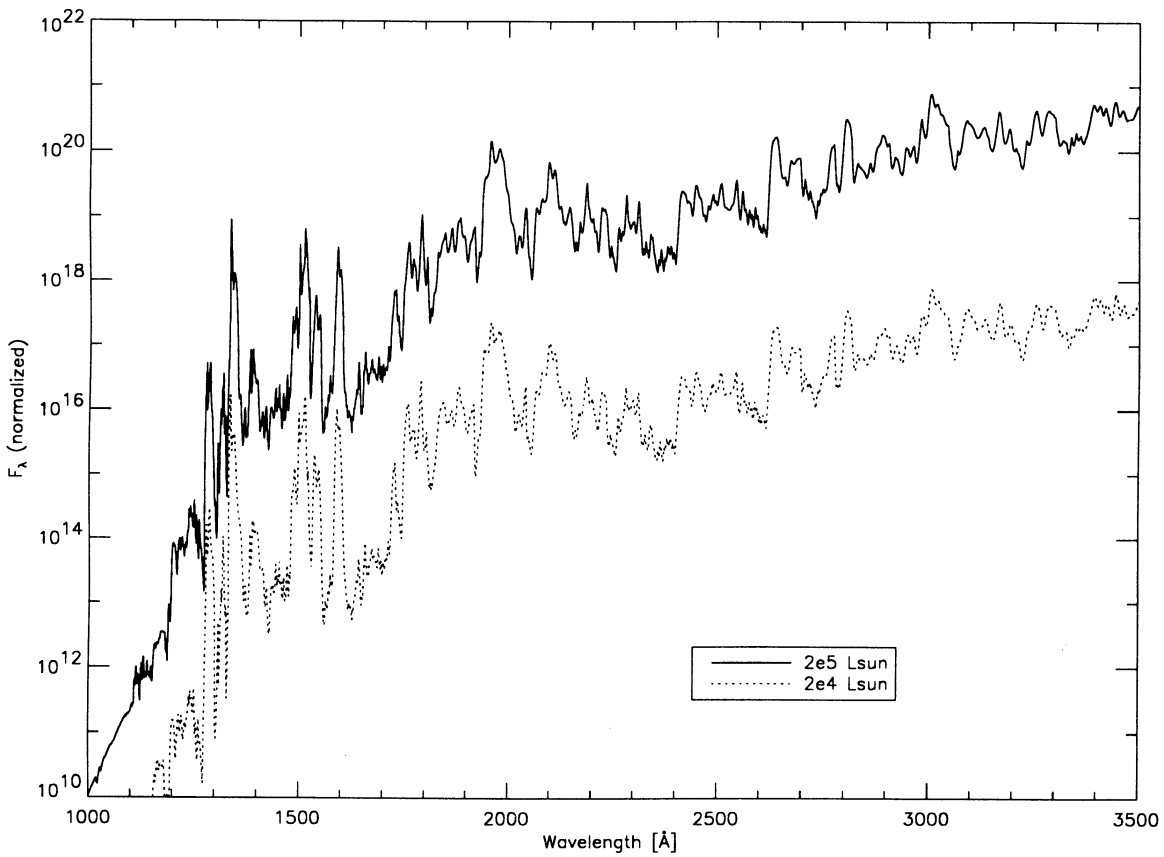


FIG. 11*b*

FIG. 11.—Effect of different luminosities on the spectra of nova atmospheres. Panel (*a*) shows the results for a model atmosphere with $T_{\rm eff} = 10{,}000$ K and $v_{\rm max} = v_\infty = 2000$ km s$^{-1}$ whereas panel (*b*) is for $T_{\rm eff} = 25{,}000$ K and $v_{\rm max} = v_\infty = 1600$ km s$^{-1}$. In each plot, the top curve is the spectrum calculated for $L = 200{,}000\ L_\odot$ whereas the bottom curve represents the results for $L = 20{,}000\ L_\odot$. The curves have been displaced relative to each other in order to make the plot clearer. Both models have the common parameter $N = 3$ and solar abundances and are self-consistently calculated with their respective luminosity.

larger luminosity also have a larger mass and mass-loss rate). The figure shows that the luminosity does *not* have a significant effect on the shape emergent spectrum, since the spectra shown in each panel of Figure 11 are nearly identical. The reason for this behavior is the general fact that the radiative transfer and the temperature structure are sensitive only to the *relative* extension of the atmosphere. For $N$ as low as 3, the geometrical extension of the atmosphere does not change significantly with the absolute radius (and therefore with the luminosity through $L \propto R^2$). The only effect is due to changes in the density of the CFR and LFR due to spherical geometry. Very large changes in density are required to produce discernible changes in the emergent spectrum. Thus, there is near a total insensitivity of the emitted spectrum to luminosity changes, much like plane-parallel stellar atmospheres.

### 3.6. *Radiation Pressure*

Although the details of the spectra are insensitive to the luminosity of the nova atmosphere, both the radiation pressure and the radiative acceleration *are* sensitive to the luminosity. In order to study the ejection mechanism of a nova shell we plot, in Figure 12, the ratio of radiative acceleration $a_{\rm rad}$ to gravity $g = a_{\rm grav}$ for a 1.25 $M_\odot$ central object at a luminosity of 70,000 $L_\odot$ (which is slightly above the classical Eddington luminosity for a 1.25 $M_\odot$ CO white dwarf) for a number of different effective temperatures and for both continua and lines + continua. If the ratio is larger than unity, then the radiative acceleration is larger than the gravity and the material can be ejected by radiation alone. Generally, $a_{\rm rad}/a_{\rm grav} > 1$ for optical depths $\tau_{\rm std} > 0.1$ at all $T_{\rm eff}$ shown in the figure. Only for $T_{\rm eff} \leq 8000$ K do we find an outer zone for which the ratio is less than unity. In these zones, however, the material has already been accelerated to speeds larger than the escape velocity and has, in fact, been ejected. In the hotter models, the radiative acceleration is always larger than gravity even for a massive white dwarf. This means that (*a*) radiative acceleration alone can eject the nova shell for the conditions shown here, and (*b*) that the velocity field inside the nova atmosphere may be changed with time due to continuous radiative acceleration. The latter effect would be able to transform a ballistic velocity field to a "wind" velocity profile.

## 4. SUMMARY AND CONCLUSIONS

Our non-LTE model atmospheres for novae show that the early evolution of a nova shell, the "optically thick" phase, can be divided into at least three very different epochs. The first and very short lived stage is the "fireball" stage, first named by Gehrz (1988) and analyzed in the UV by Hauschildt et al. (1994a). In this stage, the density gradient in the nova atmosphere is high, $N \approx 15$, and the effective temperatures are dropping from $\approx$15,000 to less than 10,000 K (lower $T_{\rm eff}$ are probable but have not yet been observed). In this stage, the

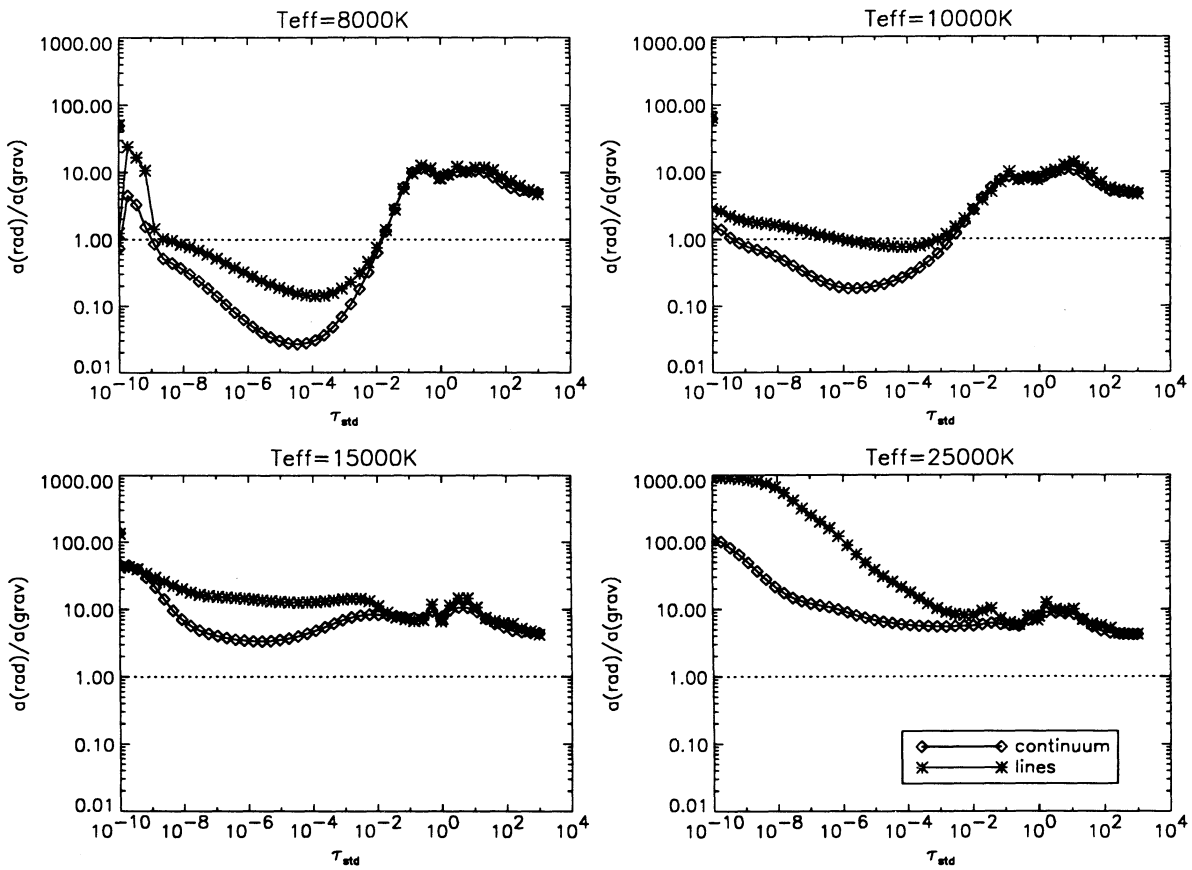


FIG. 12.—The ratio of the radiation force per mass $a_{\rm rad}$ to the gravitational acceleration $a_{\rm grav}$ (assuming $L$ = 70,000 $L_\odot$ and a 1.25 $M_\odot$ white dwarf) for four non-LTE nova atmosphere models with a ballistic (linear) velocity law and $N$ = 3. The curves annotated with diamond-shaped symbols give the results obtained by neglecting lines, whereas the curves annotated with asterisks give the results obtained including both continua and lines. $\tau_{\rm std}$ is the absorption optical depth in the continuum at $\lambda$ = 5000 Å.

nova spectrum resembles that of a SN with low velocities ($v_{max} \approx 4000$ km s$^{-1}$ for Nova V1974 Cygni 1992).

As the density and temperatures of the expanding fireball drop, the material becomes optically thin and deeper layers become visible. In this stage, the "optically thick wind phase," the atmosphere evolves to a very flat density profile, $N \approx 3$, and the LFR, as well as the CFR, has a very large geometrical extension, values of $\Delta R/R \approx 100$ in the LFR are common. The large geometrical extension causes a very large temperature gradient in the LFR, typically the electron temperatures range between 1100 K and 50,000 K for a model with $T_{eff} = 6500$ K and from 3500 K to 150,000 K for a model with $T_{eff} = 8000$ K (we emphasize that all of the regions can be visible simultaneously in the emitted spectrum). This explains the observed fact that nova spectra can show, simultaneously, lines from different ions of the same element. The structure of the atmospheres and the calculated optical spectra are very sensitive to changes of the abundances of iron, carbon, nitrogen, and oxygen, which will make abundance determinations of these elements possible. However, for reliable abundance determinations, non-LTE effects need to be included self-consistently for the elements under consideration. Consistent with the results of Pistinner et al. (1995) we also find that the synthetic spectra are insensitive to large changes in the luminosity. However, the spectra are *very* sensitive to changes in the form of the velocity profile inside the atmosphere. In terms of the classical scheme of nova spectrum classification (McLaughlin 1960), the increase in the effective temperature during the wind stage corresponds to the transition from the "premaximum spectrum" to the "diffuse enhanced spectrum."

The UV spectra of novae are totally dominated by the line blanketing of many thousands of overlapping spectral lines, mostly due to Fe II. The line blanketing changes the structure of the atmosphere, and the emitted spectrum, so radically that it must be included in the models in order to be able to reliably compare the results to observed spectra. Furthermore, the strong coupling between continua and lines, as well as the strong overlap of lines, requires a unified treatment of the radiative transfer to (at least) full first order in $v/c$ (i.e., including advection and aberration terms). Methods that separate continua and lines (e.g., the Sobolev approximation) give unreliable results. The "density" of lines in the UV is so high that practically the complete range is blocked by lines. In fact, most of the observed "emission lines" are merely gaps between "clusters" of lines, thus they are regions of transparency which have *less* opacity than the surroundig wavelength regions. In addition, the radiation fields inside the nova continuum and line-forming regions nowhere resemble blackbody or gray distributions. This condition, combined with the low densities, causes very large departures from LTE. The non-LTE radiative transfer and rate equations *must* be solved self-consistently including the effects of line blanketing in the UV and optical spectral regions. The effects of neglecting the line blanketing on the departures coefficients are enormous, as

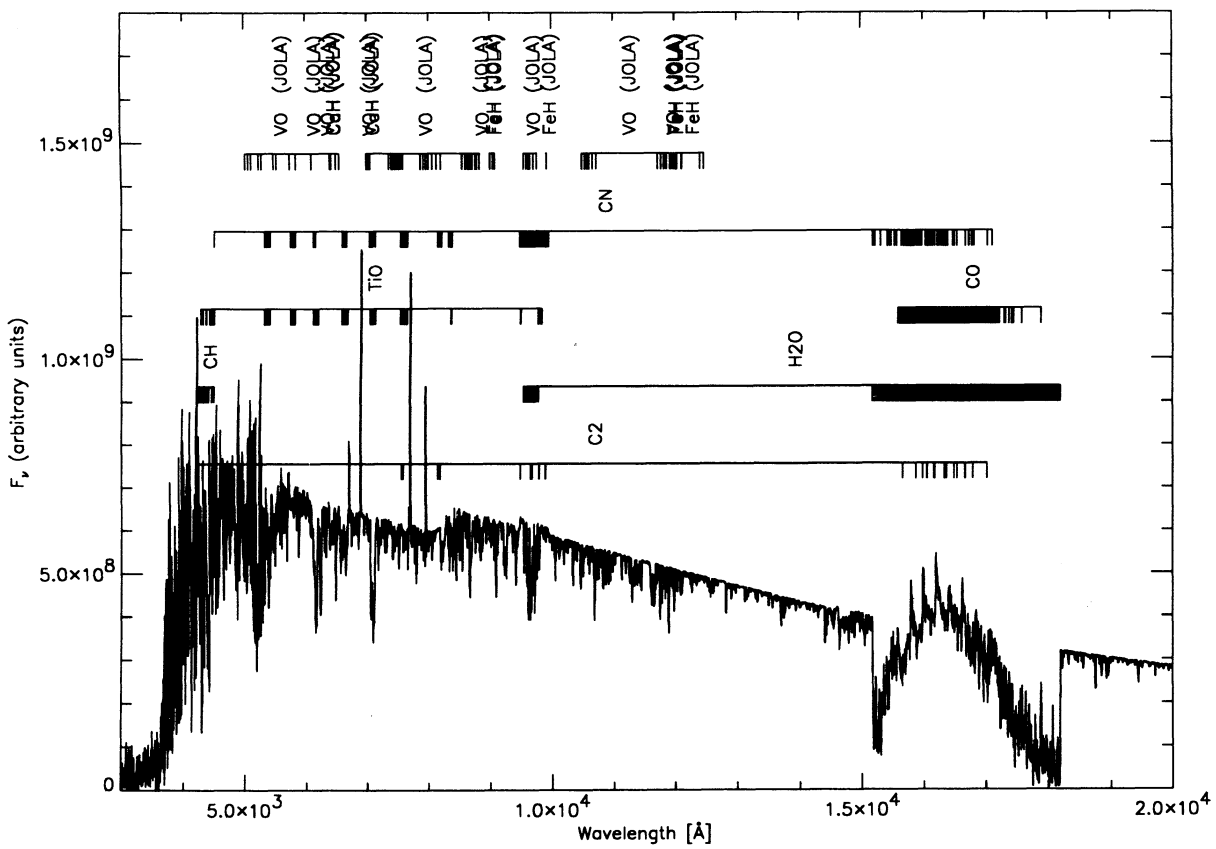


FIG. 13.—Predicted spectrum of a nova atmosphere with $T_{eff} = 5500$ K, $N = 3$, and solar abundances. The model was calculated including both atomic and molecular lines, and we have indicated the most important molecular lines/bands that are present in the spectrum. The very strong emission features in the IR are due to CO lines, whereas the absorption features at 1.4–1.5 $\mu$m and 1.94–2.0 $\mu$m are due to water vapor. In the optical and near IR, the lines of TiO and the band systems of VO are prominent.

shown by Hauschildt & Ensman (1994) for the case of SN model atmospheres.

In nova models with low effective temperatures, $T_{\rm eff} \leq$ 10,000 K, we find that molecular lines and bands are important. Our synthetic spectra for the coolest model predict the presence of molecular lines in the optical and near IR spectra (cf. Fig. 13), as has been observed in a number of historical (e.g., DQ Her) and modern (e.g., Cas 93) novae. We are currently working on detailed comparisons between models and observations for these objects. This situation could be realized in the phase between the "fireball" and the "wind" stages. Some novae show CO emission lines due to a wide manifold of transitions in their early phases (Evans et al. 1993), such as those reproduced by our models for the early observations of Cas 93 (Hauschildt et al. 1994b).

The agreement between our synthetic spectra and observed nova spectra is very good from UV to the optical. We are able to reproduce the high-resolution UV and low-resolution optical spectra of very different types of classical novae (cf. Hauschildt et al. 1994a, b for quantitative comparisons between the synthetic and observed nova spectra).

The basic physics and the modelling of early nova atmospheres is now well understood, and we are currently working on further improvements of the models (more non-LTE species) and on the analysis of those novae which have a good spectral coverage in the UV and the optical. Another important step will be to investigate the effects of density inversions (clumps) on the emitted spectrum and a more systematic investigation of the effects of different velocity fields on nova spectra is also required. Furthermore, we are currently working on a detailed treatment of the "prenebula" phase, i.e., the phase where allowed, semiforbidden and sometimes forbidden lines are simultaneously present in the observed nova spectra. This will not only require very detailed model atoms for the species showing these lines but will also extend the model atmospheres into later stages of the outburst.

It is a pleasure to thank H. Störzer, J. Krautter, G. Shaviv, and S. Pistinner for simulating discussions. We thank the referee for helpful suggestions on an earlier draft of this paper. This work was supported in part by a NASA LTSA grant to Arizona State University, by NASA grant NAGW-2999; as well as grants to G. F. Fahlman and H. B. Richer from NSERC (Canada). Some of the calculations presented in this paper were performed at the San Diego Supercomputer Center (SDSC), supported by the NSF, and at the NERSC, supported by the US Department of Energy, we thank them for a generous allocation of computer time.

## APPENDIX

## SOLUTION OF THE RATE EQUATIONS

We introduce the "rate operator" $[R_{ij}]$ for upward transitions in analogy with the $\Lambda$-operator. $[R_{ij}]$ is defined so that

$$R_{ij} = [R_{ij}][n] \; . \tag{A1}$$

Here, $[n]$ denotes the "population density operator," which can be considered as the vector of the population densities of all levels at all points in the medium under consideration. Physically, the operator $[R_{ij}]$ describes the influence of any level $k$ on the radiative rate $R_{ij}$ of the transition $i \rightarrow j$. The radiative rates are (linear) functions of the mean intensity $J$, which is given by $J(\lambda) = \Lambda(\lambda)S(\lambda)$, where $S = \eta(\lambda)/\chi(\lambda)$ is the source function. Using the $\Lambda$-operator, we can write $[R_{ij}][n]$ as

$$[R_{ij}][n] = \frac{4\pi}{hc} \int \alpha_{ij}(\lambda)\Lambda(\lambda)S(\lambda)\lambda \, d\lambda \; . \tag{A2}$$

We rewrite the $\Lambda$-operator as

$$\Lambda(\lambda) = \Psi(\lambda)[1/\chi(\lambda)] \; , \tag{A3}$$

where we have introduced the $\Psi$-operator and $[1/\chi(\lambda)]$ is the diagonal operator of multiplying by $1/\chi(\lambda)$. Using the $\Psi$-operator, we can write $[R_{ij}]$ as

$$[R_{ij}][n] = \frac{4\pi}{hc} \int \alpha_{ij}(\lambda)\Psi(\lambda)\eta(\lambda)\lambda \, d\lambda \; , \tag{A4}$$

where $\eta(\lambda)$ is a function of the population densities and the background emissivities. Using $\chi(\lambda) = \Sigma_{i<j}\kappa_{ij}(\lambda) + \tilde{\kappa}(\lambda) + \tilde{\sigma}(\lambda)$, we can write $\eta(\lambda)$ as

$$\eta(\lambda) = \sum_{i<j} \eta_{ij}(\lambda) + \tilde{\eta}(\lambda) \equiv [E(\lambda)][n] \; , \tag{A5}$$

where we have defined the linear and diagonal operator $[E(\lambda)]$.

With this $[E(\lambda)]$-operator, we write $[R_{ij}][n]$ in the form

$$[R_{ij}][n] = \frac{4\pi}{hc} \left[ \int_0^\infty \alpha_{ij}(\lambda)\Psi(\lambda)E(\lambda)\lambda \, d\lambda \right][n] \; . \tag{A6}$$

The corresponding expression for the emission rate-operator $[R_{ij}]$ is given by

$$[R_{ji}][n] = \frac{4\pi}{hc} \int_0^\infty \alpha_{ji}(\lambda)\left\{\frac{2hc^2}{\lambda^5} + \Psi(\lambda)[E(\lambda)][n]\right\} \exp\left(-\frac{hc}{k\lambda T}\right)\lambda \, d\lambda \; . \tag{A7}$$

As in the case of the two-level atom, a simple Λ-iteration scheme will converge much too slowly to be useful for most cases of practical interest. Therefore, we split the rate operator, analogously to splitting the Λ-operator, by $[R_{ij}] = [R^*_{ij}] + ([R_{ij}] - [R^*_{ij}]) \equiv [R^*_{ij}] + [\Delta R_{ij}]$ (analog for the downward radiative rates), where $[R^*_{ij}]$ is the "approximate rate-operator." We then rewrite the rate $R_{ij}$ as

$$R_{ij} = [R^*_{ij}][n_{\rm new}] + [\Delta R_{ij}][n_{\rm old}] \tag{A8}$$

and analogously for the downward radiative rates. In equation (A8), $[n_{\rm old}]$ denotes the current (old) population densities, whereas $[n_{\rm new}]$ are the updated (new) population densities to be calculated. The $[R^*_{ij}]$ and $[R^*_{ji}]$ are linear functions of the population density operator $[n_k]$ of any level $k$, due to the linearity of $\eta$ and the usage of the Ψ-operator instead of the Λ-operator.

If we insert equation (A8) into equation (6) we obtain the following system for the new population densities:

$$\begin{aligned}
&\Sigma_{j<i} n_{j,\rm new}[R^*_{ji}][n_{\rm new}] - n_{i,\rm new}\left\{\Sigma_{j<i}\left(\frac{n^*_j}{n^*_i}\right)[R^*_{ij}][n_{\rm new}] + \Sigma_{j>i}[R^*_{ij}][n_{\rm new}]\right\} \\
&\quad + \Sigma_{j>i} n_{j,\rm new}\left(\frac{n^*_i}{n^*_j}\right)[R^*_{ji}][n_{\rm new}] + \Sigma_{j<i} n_{j,\rm new}([\Delta R_{ji}][n_{\rm old}] + C_{ji}) \\
&\quad - n_{i,\rm new}\left\{\Sigma_{j<i}\left(\frac{n^*_j}{n^*_i}\right)([\Delta R_{ij}][n_{\rm old}] + C_{ji}) + \Sigma_{j>i}([\Delta R_{ij}][n_{\rm old}] + C_{ij})\right\} + \Sigma_{j>i} n_{j,\rm new}\left(\frac{n^*_i}{n^*_j}\right)([\Delta R_{ji}][n_{\rm old}] + C_{ij}) = 0 .
\end{aligned} \tag{A9}$$

Due to its construction, the $[R^*_{ij}]$ operator contains information about the influence of a particular level on *all* radiative transitions. Therefore, we are able to treat the complete multilevel non-LTE radiative transfer problem including active continua and overlapping lines. The $[E(\lambda)]$ operator, at the same time, gives us information about the strength of the coupling of a radiative transition to all levels. This information may be used to include or neglect certain couplings *dynamically* during the iterative solution of equation (A9). We construct our $[R^*_{ij}]$ operator in the same way as the ALO for the radiative transfer, i.e., we use the exact bands of the discretized rate operator. As in the case of the radiative transfer, this leads to rapid convergence, see Hauschildt (1993) for details. We use the method outlined above for the solution of the non-LTE radiative transfer and rate equations in our nova model atmospheres. It is very reliable and converges very well even for the extreme conditions found in nova atmospheres.

## REFERENCES


Allard, F. 1990, Ph.D. thesis, Univ. of Heidelberg
Allard, F., & Hauschildt, P. H. 1995, ApJ, 445, 433
Allard, F., Hauschildt, P. H., Miller, S., & Tennyson, J. 1994, ApJ, 426, L39
Allen, C. W. 1973, Astrophysical Quantities (3d ed.; London: Athlone Press)
Auer, L. H., & Mihalas, D. 1973, ApJ, 184, 151
Bath, G. T., & Shaviv, G. 1976, MNRAS, 197, 305
Cannon, C. J. 1973, J. Quant. Spectros. Rad. Transf., 13, 627
Cunto, W., & Mendoza, C. 1992, Topbase Users Guide, Technical Report CSC-01-92, IBM (Caracas; Venezuela Scientific Center)
Drawin, H. W. 1961, Z. Phys., 164, 513
Evans, A., et al. 1993, IAU Circ., No. 5916
Gehrz, R. D. 1988, ARA&A, 26, 377
Goorvitch, D. 1994, ApJS, 95, 535
Hauschildt, P. H. 1992a, J. Quant. Spectros. Rad. Transf., 47, 433
———. 1992b, ApJ, 398, 224
———. 1993, J. Quant. Spectros, Rad. Transf., 50, 301
Hauschildt, P. H., & Baron, E. 1995, J. Quant. Spectros. Rad. Transf., submitted
Hauschildt, P. H., Best, M., & Wehrse, R. 1991, A&A, 247, L21
Hauschildt, P. H., & Ensman, L. M. 1994, ApJ, 424, 905
Hauschildt, P. H., Starrfield, S., Austin, S. J., Wagner, R. M., Shore, S. N., & Sonneborn, G. 1994a, ApJ, 422, 831
Hauschildt, P. H., Starrfield, S., Shore, S. N., Gonzales-Riestra, R., Sonneborn, G., & Allard, F. 1994b, AJ, 108, 1008
Hauschildt, P. H., Störzer, H., & Baron, E. 1994c, J. Quant. Spectros. Rad. Transf., 51, 875
Hauschildt, P. H., & Wehrse, R. 1991, J. Quant. Spectros. Rad. Transf., 46, 81
Hauschildt, P. H., Wehrse, R., Starrfield, S., & Shaviv, G. 1992, ApJ, 393, 307
Hertz, H. 1969, Zs. Nat., 24a, 1937
Jørgensen, U. G. 1994, A&A, 284, 179
Jørgensen, U. G., & Larsson, A&A, 238, 424
Kudritzki, R. P., & Hummer, D. G. 1990, ARA&A, 28, 303
Kurucz, R. L. 1993a, Atomic Data for Opacity Calculations, Kurucz CD-ROM, No. 1
———. 1993b, Molecular Data for Opacity Calculations, Kurucz CD-ROM, No. 15
Mathisen, R. 1984, Photo Cross Sections for Stellar Atmosphere Calculations—Compilation of References and Data, Inst. of Theoret. Astrophys. Univ. of Oslo, Publ. Ser., No. 1.
McLaughlin, D. B. 1960, in Stars and Stellar Systems, Vol. 6, Stellar Atmospheres, ed. J. L. Greenstein (Chicago: Univ. of Chicago Press), 585
Mihalas, D. 1978, Stellar Atmospheres (2d ed.; San Francisco: Freeman)
Mihalas, D., Kunasz, P. B., & Hummer, D. G. 1976, ApJ, 206, 515
Mihalas, D., & Weibel-Mihalas, B. 1984, Foundations of Radiation Hydrodynamics (Oxford: Oxford Univ. Press)
Moore, C. E. 1971, Atomic Energy Levels, Vol. I, Tech. Rep., NSRDS-NBS 35, National Bureau of Standards
Murphy, P. W. 1968, J. Opt. Soc. Am., 58, 1200
Olson, G. L., Auer, L. H., & Buchler, J. R. 1987, J. Quant. Spectros. Rad. Transf., 38, 431
Pistinner, S., Shaviv, G., Hauschildt, P. H., & Starrfield, S. 1995, ApJ, in press
Rothman, L. S., et al. 1992, J. Quant. Spectros. Rad. Transf., 48, 469
Scharmer, G. B. 1984, in Methods in Radiative Transfer, ed. W. Kalkofen (Cambridge: Cambridge Univ. Press), 173
Shara, M. 1989, PASP, 101, 5
Sharpton, F. A., St. John, R. M., Lin, C. C., & Fajen, F. E. 1970, Phys. Rev., A2, 1305
Starrfield, S. 1989, in Classical Novae, ed. M. F. Bode & A. Evans (New York: Wiley), 39
Vajnshtejn, L. A., & Minaeva, L. 1968, J. Appl. Spectr., 9, 684
Van Regemorter, H. 1962, ApJ, 136, 906